

TSUNAMI INUNDATION MAP FOR THE VILLAGE OF NIKOLSKI, ALASKA

D.J. Nicolsky, E.N. Suleimani, and R.D. Koehler



Nikolski village at the head of Nikolski Bay, Umnak Island, Alaska. Photo by Rich Koehler.



Published by
STATE OF ALASKA
DEPARTMENT OF NATURAL RESOURCES
DIVISION OF GEOLOGICAL & GEOPHYSICAL SURVEYS
2016



TSUNAMI INUNDATION MAP FOR THE VILLAGE OF NIKOLSKI, ALASKA

D.J. Nicolsky, E.N. Suleimani, and R.D. Koehler

Report of Investigations 2016-7

State of Alaska
Department of Natural Resources
Division of Geological & Geophysical Surveys



STATE OF ALASKA

Bill Walker, *Governor*

DEPARTMENT OF NATURAL RESOURCES

Andy Mack, *Commissioner*

DIVISION OF GEOLOGICAL & GEOPHYSICAL SURVEYS

Steve Masterman, *State Geologist and Director*

Publications produced by the Division of Geological & Geophysical Surveys (DGGS) are available for free download from the DGGS website (www.dggs.alaska.gov). Publications on hard-copy or digital media can be examined or purchased in the Fairbanks office:

Alaska Division of Geological & Geophysical Surveys

3354 College Rd., Fairbanks, Alaska 99709-3707

Phone: (907) 451-5010 Fax (907) 451-5050

dggspubs@alaska.gov

www.dggs.alaska.gov

Alaska State Library
State Office Building, 8th Floor
333 Willoughby Avenue
Juneau, Alaska 99811-0571

Alaska Resource Library & Information
Services (ARLIS)
3150 C Street, Suite 100
Anchorage, Alaska 99503-3982

CONTENTS

INTRODUCTION	1
PROJECT BACKGROUND: REGIONAL AND HISTORICAL CONTEXT	2
Setting	2
Seismic and Tsunami History	2
Landslide-Generated Tsunami Hazards	2
METHODOLOGY AND DATA	2
Grid Development and Data Sources	2
Numerical Model of Tsunami Propagation and Runup	4
Modeling of the March 11, 2011 Tohoku Tsunami	4
Tsunami Sources	6
Sensitivity Study	6
Earthquake Scenarios	6
Scenario 1: M_w 9.1 earthquake in the Fox Islands region, based on hypothetical cases C and D	6
Scenario 2: M_w 9.1 earthquake in the Fox Islands region, based on hypothetical cases D and E	9
Scenario 3: M_w 9.1 earthquake in the Fox Islands region, based on hypothetical case C	9
Scenario 4: M_w 9.0 earthquake according to the SAFRR project	9
Scenario 5: M_w 9.0 SAFRR-type earthquake in the Samalga Pass region	9
Scenario 6: M_w 9.2 East Aleutian earthquake	9
Scenario 7: M_w 9.25 East Aleutian earthquake	9
Scenario 8: M_w 9.1 earthquake, Fox Islands region	14
Scenario 9: Rupture of the Cascadia zone, including the entire megathrust between British Columbia and northern California	14
Scenario 10: Rupture of the tensional outer-rise part of the subduction plate south of the trench in the Umnak Island area	14
MODELING RESULTS	14
Time Series	15
Sources of Errors and Uncertainties	15
SUMMARY	15
ACKNOWLEDGMENTS	16
REFERENCES	19

FIGURES

Figure 1. Map of the western tip of the Alaska Peninsula and eastern Aleutian Islands, showing the Alaska–Aleutian subduction zone and the rupture zones of the 1946, 1948, 1957, 1986, and 1996 earthquakes	1
2. Map of the southwestern tip of Umnak Island and nesting of the Levels 2–4 bathymetry/topography grids for numerical modeling of tsunami propagation and runup	3
3. Locations of RTK (real-time kinetic) GPS measurements in Nikolski	5
4. Observed water-level dynamics in Nikolski and fitted GPS measurements of water level in the MHHW datum	5
5. Comparison of modeled and observed water-level dynamics at the tide station in Nikolski during the March 11, 2011, Tohoku tsunami	5

FIGURES, CONTINUED

Figure	6.	Assumed slip distribution along the plate interface for cases A–E, modeling a Mw 8.2 rupture across Samalga Pass	7
	7.	Computed vertical ground-surface deformation related to cases A–E	8
	8.	Modeled water-level dynamics in Mueller Cove adjacent to Nikolski for ground-surface deformations.....	9
	9.	Proposed slip distribution along the plate interface for Scenarios 1, 2, 3, and 5 based on selected hypothetical cases.....	10
	10.	Computed vertical ground-surface deformation related to proposed slip distributions and an outer-rise event.....	12
	11.	Modeled potential inundation in Nikolski by tectonic waves for all scenarios	16
	12.	Modeled time series of water level in Mueller Cove for scenarios 1–10	17
	13.	Modeled time series of water level along the Pacific coast of Umnak Island for scenarios 1–10.....	18

TABLES

Table	1.	Nested grids used to compute propagation of tsunami waves generated in the Pacific Ocean to the community of Nikolski.	4
	2.	Fault parameters for the hypothetical tensional Mw 8.6 outer-rise earthquake (scenario 10)	13
	3.	All hypothetical scenarios used to model tsunami runup in Nikolski	14

APPENDICES

APPENDIX A	21	
Figure A-1.	Locations of time series points on western Umnak Island (A) and in the village of Nikolski (B)	21
A-2.	Time series of water level and velocity at selected locations in Nikolski and the Pacific coast of Umnak Island for scenarios 1, 5, 6, and 7	22
A-3.	Time series of water level and velocity at selected offshore locations in Mueller Cove and along the Pacific coast of Umnak Island for scenarios 4, 9, and 10.....	28
Table A-1.	Longitude and latitude locations of the time series points in Nikolski.....	29

SHEETS

Sheet	1.	Maximum estimated tsunami inundation, Nikolski, Alaska
-------	----	--

TSUNAMI INUNDATION MAP FOR THE VILLAGE OF NIKOLSKI, ALASKA

D.J. Nicolsky¹, E.N. Suleimani¹, and R.D. Koehler²

ABSTRACT

Potential tsunami hazard for the Umnak Island community of Nikolski is evaluated by numerically modeling the extent of inundation from tsunami waves generated by hypothetical earthquake sources. Worst-case hypothetical scenarios are defined by analyzing results of a sensitivity study of the tsunami dynamics related to various slip distributions along the Aleutian megathrust. The worst-case scenarios for Nikolski are thought to be thrust earthquakes in the Umnak Island region with their greatest slip at 10–30 km (6.2–19 mi) depth. We also consider Tohoku-type ruptures and an outer-rise rupture in the area of Umnak Island. The maximum predicted water depth on Main Street is about 15 m (49 ft), while the maximum current velocity in Mueller Cove could exceed 8 m/s (15 kt) and significant wave action could continue for at least 8 hours after the earthquake. Results presented here are intended to provide guidance to local emergency management agencies in tsunami inundation assessment, evacuation planning, and public education to mitigate future tsunami hazards.

INTRODUCTION

The Aleutian Islands of Akutan, Unalaska, and Unimak are on top of the Alaska–Aleutian subduction zone and have been shaped by volcanic eruptions, earthquakes, and erosion processes over the course of millions of years. Subduction of the Pacific plate under the North American plate has resulted in numerous tsunamigenic earthquakes and has the highest potential to generate tsunamis in Alaska (Dunbar and Weaver, 2008). Nearly the entire Aleutian megathrust has ruptured in the twentieth century, causing great ($M > 8$) earthquakes in 1938, 1946, 1957, 1964, and 1965 (Carver and Plafker, 2008, and references therein). Additionally, several $M 7.9$ events have ruptured the western end of the

subduction zone including events in 1986, 1996, and 2014 (Boyd and Nabelek, 1988; AEC, 2015). The most recent earthquakes that triggered great tsunamis along the coast of Umnak Island occurred on April 1, 1946, and March 9, 1957, with tsunami runup of 12.2 m (40 ft) and 22.9 m (75 ft) along the Pacific coast of the island, respectively (Lander, 1996). Locations of the 1946 and 1957 events relative to Umnak Island are shown in figure 1.

During the 1946 event, observers reported that water withdrew from Nikolski Bay and that a wave ran up over the bank and washed driftwood up onto the ice of a lake a quarter of a mile from the Bering Sea coast (Lander, 1996).

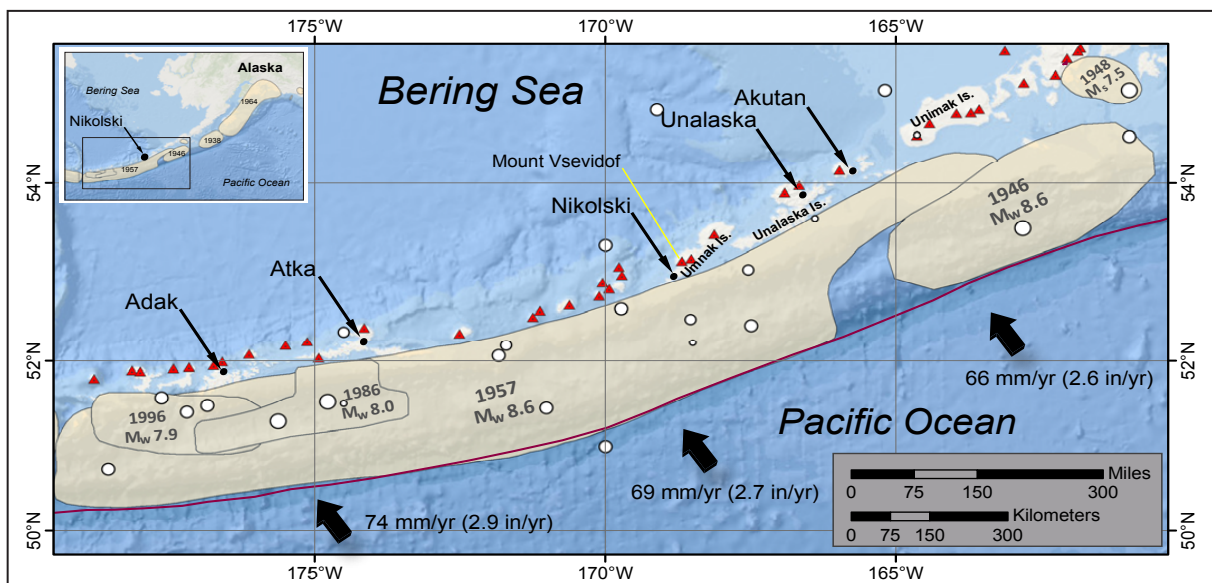


Figure 1. Map of the western tip of the Alaska Peninsula and eastern Aleutian Islands, showing the Alaska–Aleutian subduction zone (heavy red line) and the rupture zones of the 1946, 1948, 1957, 1986, and 1996 earthquakes (light shaded areas). Red triangles indicate historically active volcanoes. White circles are epicenters of historic earthquakes (National Geophysical Data Center [NGDC], <http://maps.ngdc.noaa.gov/arcgis/services>). The spatial extent of the map is shown by the black rectangle in the inset map.

¹Geophysical Institute, University of Alaska, P.O. Box 757320, Fairbanks, Alaska 99775-7320; djnicolky@alaska.edu

²Alaska Division of Geological & Geophysical Surveys, 3354 College Road, Fairbanks, AK 99709-3707; now at Nevada Bureau of Mines and Geology, Mackay School of Earth Science and Engineering, University of Nevada, Reno, 1664 North Virginia Street, MS 178, Reno, NV 89557

No records exist for the 1957 tsunami in Nikolski. Witter and others (2014) documented drift logs stranded up to 23 m (75.5 ft) above sea level and described nine sand sheets in the Driftwood Bay area (fig. 2A). Based on these observations, Witter and others (2014) inferred the occurrence of repeated high tsunamis at Umnak Island. The potential future occurrence of earthquakes and tsunamis necessitates the development of inundation and tsunami evacuation maps for use in tsunami risk mitigation. In this report, we provide an analysis of the tsunami hazard and develop tsunami inundation maps for the village of Nikolski³.

The methodologies used to develop tsunami inundation maps are described in detail in multiple other publications and descriptions are not duplicated in this report. Reports by Suleimani and others (2010, 2013, 2015) and Nicolsky and others (2011a, 2013, 2014, 2015) include full descriptions of the procedure.

PROJECT BACKGROUND: REGIONAL AND HISTORICAL CONTEXT

SETTING

The village of Nikolski is on Umnak Island at 52°56' N, 168°51' W, or about 1,450 km (~900 mi) southwest of Anchorage, and 3,300 km (2,050 mi) northwest of Seattle (fig. 1). The 2010 U.S. Census recorded the population as 18. Settlements on Umnak Island and nearby Anangula Island have a history dating back thousands of years (McCartney and Turner, 1966; Aigner, 1974, 1976). According to William and Marsh (1951) the village of Chaluka (the old Unangan name for Nikolski) has been continuously occupied for the last 4,000 years. Before the arrival of Europeans, it comprised about 22 village sites scattered around Umnak Island, with a total population of about 2,000. During the Russian period, Nikolski served as sea otter hunting grounds and was the location of the Unangan rebellion in 1763–1764. A sheep ranch was established on the island in the 1920s; sheep, cattle, and horses continue to roam and graze much of the land.

A community center, clinic, school and teachers' housing, church, lodge, and more than 20 other buildings are established in the village. Most local residents support themselves by working outside the village at crab canneries and on processing ships (Aleutian Pribilof Island Association, 2015). Although Nikolski has a 1,070 m (3,510 ft) unlighted gravel runway that provides passenger, mail, and cargo service, the village lacks a harbor and dock facilities for ships. Barges deliver cargo once or twice a year. Goods and passengers are lightered 4.8 km (3.0 mi) to the beach (DCCED/DCRA, 2013). As in many other coastal villages, much of the economic activity and infrastructure such as fuel tanks and roads are on or near the coast—a potential tsunami inundation area.

³An additional concern in the Umnak Island area is Mount Vsevidof, which is near the community of Nikolski and last erupted in 1957, presumably triggered by the earthquake (Lander, 1996). Although the 1957 eruption lasted for only one day, an erupting volcano in the area of potential inundation can hinder post-tsunami relief efforts and could be considered in future multi-hazard scenarios.

⁴Guidelines and best practices for tsunami inundation modeling for evacuation planning state that the modeling should add value to mapping products (National Tsunami Hazard Mapping Program [NTHMP], 2010).

SEISMIC AND TSUNAMI HISTORY

Numerous earthquakes and tsunamis have likely affected the Umnak and Unalaska Islands (Nicolsky and others [2015], fig. 5). A description of these events as well as the seismic and tsunami history for nearby Unalaska Island are provided in Nicolsky and others (2015); however, no reports or eye-witness accounts of these events in Nikolski prior to 1946 are available. Given the close proximity of Umnak Island to Unalaska Island, the two islands likely experienced similar earthquake and tsunami histories.

LANDSLIDE-GENERATED TSUNAMI HAZARDS

As in the tsunami modeling study for Unalaska and Akutan (Nicolsky and others, 2015), we do not model tsunamis generated by any mass failures due to insufficient data on the locations and volumes of these potential hazards⁴. Nicolsky and others (2013; 2015) and Suleimani and others (2015) provide detailed reviews of the primary causes and typical geomorphic settings of submarine slumps.

METHODOLOGY AND DATA

GRID DEVELOPMENT AND DATA SOURCES

We employ a series of nested bathymetry/topography grids (fig. 2) generated from a variety of sources to create a detailed map of potential tsunami inundation in Nikolski. The coarsest grid, with 2-arc-minute (approximately 2 km [~1.2 mi]) resolution, spans the central and northern Pacific Ocean. We use three intermediate grids between the coarsest- and highest-resolution grids (table 1). Note that the 2-arc-minute, 8-arc-second, and 24-arc-second-resolution grids (Levels 0, 1, and 2) are the same as in modeling of the potential tsunami inundation for Unalaska/Dutch Harbor (Nicolsky and others, 2015). On the Bering Sea side of Umnak Island, the highest-resolution grid for Nikolski (Level 4) covers the village of Nikolski, Mueller Cove, Nikolski Bay, the southern part of Anangula Island, and Cape Starr. On the Pacific side of Umnak Island, this grid includes the area around Cape Udak and Driftwood Bay. The lateral extent of the high-resolution grid is shown by a red rectangle in figure 2A. The spatial resolution of the high-resolution grid cells, with 16.5 × 16.4 m (54.1 × 53.8 ft) dimensions, satisfies National Oceanic and Atmospheric Administration (NOAA) minimum recommended requirements for computation of tsunami inundation (National Tsunami Hazard Mapping Program [NTHMP], 2010).

To develop high-resolution and 8/3-arc-second-resolution grids (Levels 3 and 4), shoreline, bathymetric, and topographic digital datasets were obtained from various agencies.

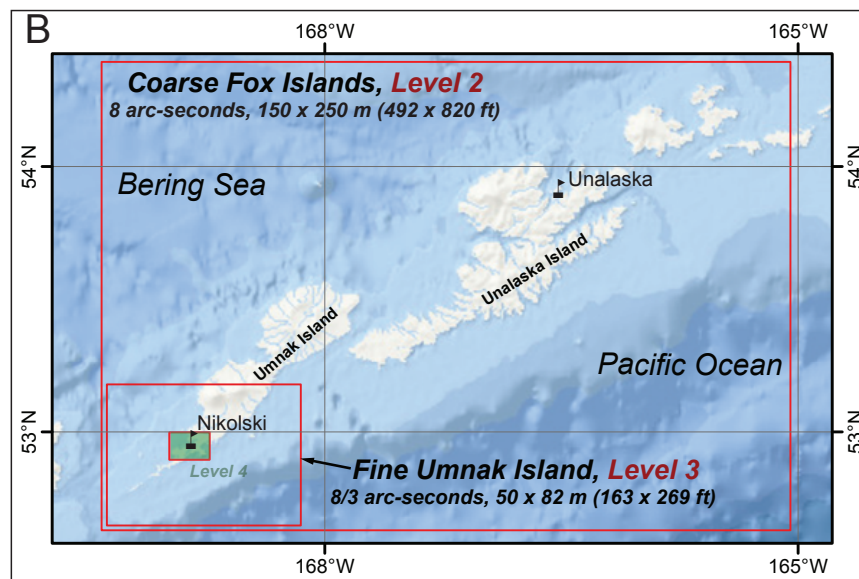
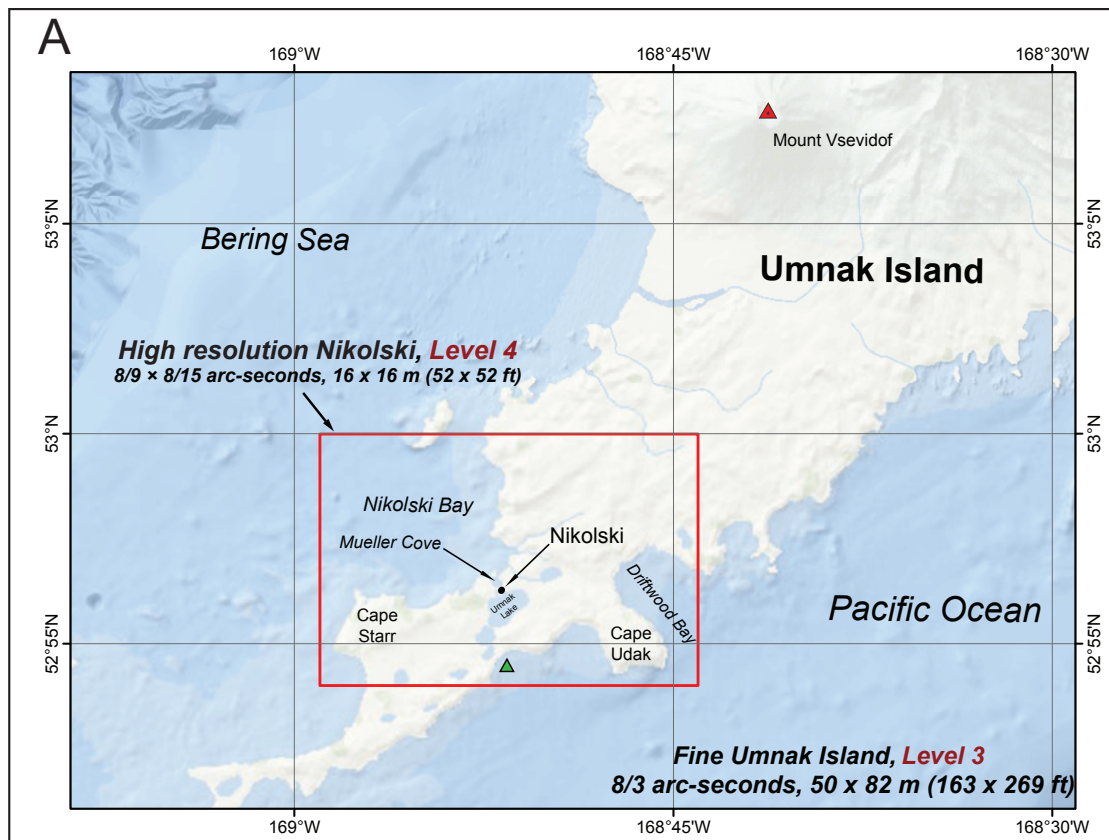


Figure 2. (A) Map of the southwestern tip of Umnak Island. Red rectangle marks spatial extent of the high-resolution grid used to simulate tsunami runup around the village of Nikolski. The location with recorded water-level dynamics on the Pacific coast of Umnak Island is marked by a green triangle. (B) Nesting of Levels 2–4 bathymetry/topography grids for numerical modeling of tsunami propagation and runup. The nesting of Levels 0 and 1 grids is shown in Nicolsky and others (2015, fig. 9). The spatial extent of each embedded grid (marking areas of increasing grid refinement) is shown by red rectangles.

Lateral extents and nesting of the Level 3 and Level 4 grids are shown in figure 2B. The bathymetric datasets include NOS hydrographic surveys, multi-beam swath sonar surveys, and the NGDC/NOAA ETOPO1 Global Relief Model. The topographic dataset was obtained from USGS National Elevation Dataset (NED), NASA Space Shuttle Radar Topography Mission (SRTM), NASA Advanced Spaceborne Thermal Emission and Reflection Radiometer (ASTER), and Alaska Division of Community and Regional Affairs (DCRA). All data were shifted to World Geodetic System 1984 (WGS 84) horizontal and Mean Higher High Water (MHHW) vertical datums. The data sources and methodology used to develop high-resolution and 8/3-arc-second DEMs are described in detail by Lim and others (2011) and Beasley and others (2014).

Accuracy of the high-resolution DEM was initially controlled by the DCRA elevation dataset (survey data with the original Geoid 99 vertical datum), which had an unknown accuracy. Because conversion of the DCRA datum to the MHHW datum could result in some vertical error, prediction of the potential tsunami inundation using those data can be invalid. Hence, this topographic dataset was augmented with a real-time kinematic (RTK) GPS survey conducted April 4–6, 2014, along nearshore areas in Nikolski. The locations of GPS measurements in Nikolski are shown in figure 3, and a comparison of the GPS-estimated and NOAA-observed tide dynamics is shown in figure 4.

We check the accuracy of our conversion of the GPS data to the MHHW level by measuring the height of the tidal station disk 2450E 2006 in Nikolski. According to the NOAA website (<http://tidesandcurrents.noaa.gov>) the disk is 4.685 m (15.371 ft) above the MHW, or 4.582 m (15.033 ft) above the MHHW. After measuring the height of this disk during the GPS survey and converting to the MHHW datum, we calculate that the disk is 4.498 m (14.76 ft) above the MHHW. The difference of less than 0.1 m (0.33 ft) between the NOAA stamping and our measurement demonstrates that the conversion of the GPS measurements to the MHHW level provides sub-meter accuracy. Because we could not find a suitable benchmark to verify horizontal positioning of the collected GPS measurements (WGS84 horizontal datum), we

assume that their horizontal accuracy is approximately 3–5 m (10–16 ft) as defined by the initial positioning error of the base station (Leica Geosystems AG, 2002) and is well below the spatial resolution of the Level 4 grid. The converted GPS survey has been provided to the National Geophysical Data Center (NGDC), where the high-resolution DEM of Unalaska/Dutch Harbor and adjacent areas has been developed.

NUMERICAL MODEL OF TSUNAMI PROPAGATION AND RUNUP

To estimate tsunami propagation and runup for Nikolski, we use the same numerical model employed in the tsunami inundation study of Unalaska and Akutan (Nicolosky and others, 2015). All model runs were conducted with the bathymetric data corresponding to the MHHW tide level in Nikolski.

MODELING OF THE MARCH 11, 2011 TOHOKU TSUNAMI

To test the accuracy of the grid nesting, we completed a model verification study of the Tohoku tsunami of March 11, 2011. Using the methods of Nicolosky and others (2015) we determined that the arrival times of the computed wave at the DART buoys and Nikolski occur sooner than the observed wave. Figure 5 shows the comparison of the computed and measured water-level dynamics at the Nikolski tidal station. The Tohoku tsunami of March 11, 2011, produced a 0.84 m (2.76 ft) wave in Nikolski (NOAA/WDS Global Historical Tsunami Database), whereas the simulation predicts a 1.28 m (4.20 ft) wave. Note that the time delay between the computed and measured water-level dynamics is $\delta T = 9$ minutes. A similar time lag is observed by Tang and others (2012). The probable cause of this increase is errors in the bathymetry and some dispersion effects.

The far-field Tohoku tsunami did not result in a significant wave in Nikolski due to its distance from the Fox Islands and directivity patterns of the energy propagation. However, other distant events could produce larger wave heights in Nikolski and should not be dismissed without proper evaluation. Additional information about the tsunami dynamics

Table 1. Nested grids used to compute propagation of tsunami waves generated in the Pacific Ocean to the community of Nikolski. The high-resolution grid is used to compute the inundation. Note that the grid resolution in meters is not uniform: the first dimension is the longitudinal grid resolution and the second is the latitudinal resolution. Measurements also vary across each grid and are given for a reference location near Fox Islands to illustrate relative grid fineness. Grids for Levels 0, 1, and 2 are the same as those used to model potential tsunami inundation in Unalaska/Dutch Harbor (Nicolosky and others, 2015).

Grid name	Resolution		East–West boundaries	North–South boundaries
	arc-seconds	meters (near Fox Islands)		
Level 0, Northern Pacific	120 × 120	≈ 1,850 × 3,700	120°00' E–100°00' W	10°00' N–65°00' N
Level 1, Eastern Aleutians	24 × 24	≈ 430 × 740	171°58' W–157°02' W	52°00' N–57°28' N
Level 2, Coarse resolution Fox Islands	8 × 8	≈ 150 × 250	169°25' W– 165°03' W	52°37' N–54°23' N
Level 3, Fine resolution Umnak Island	8/3 × 8/3	≈ 48 × 82	169°24' W– 168°09' W	52°38' N–53°11' N
Level 4, High resolution Nikolski	8/9 × 8/15	≈ 16 × 16	168°59' W–168°44' W	52°54' N–53°00' N

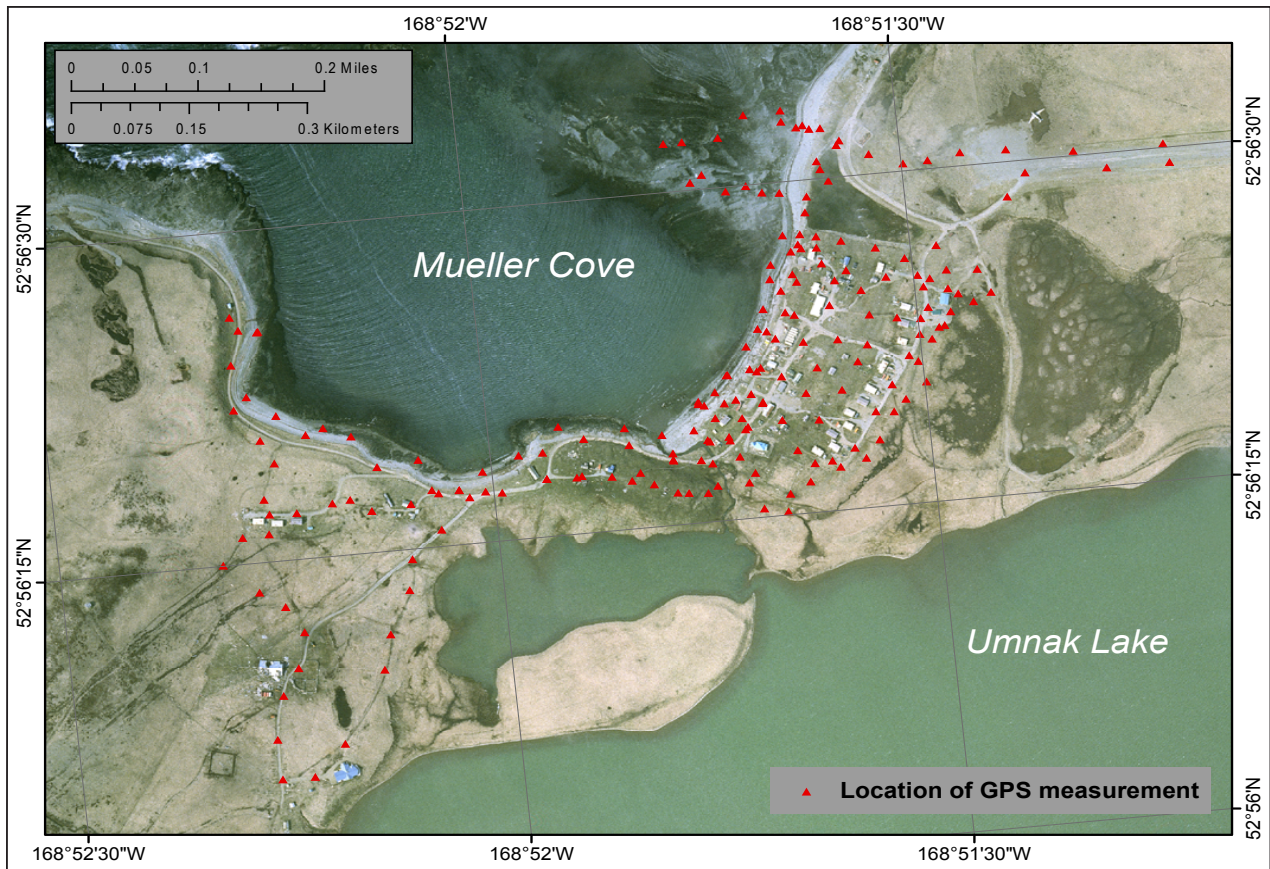


Figure 3. Locations of RTK (real-time kinetic) GPS measurements in Nikolski.

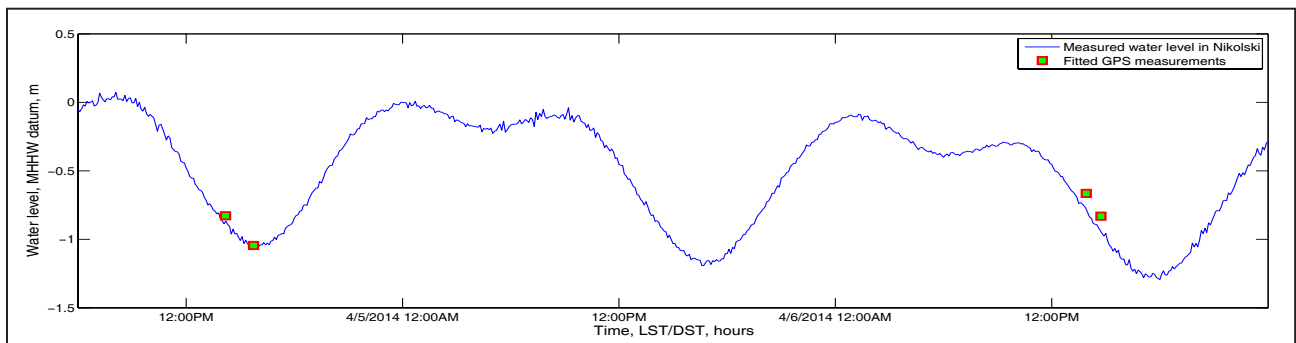


Figure 4. Observed water-level dynamics in Nikolski and fitted GPS measurements of water level in the MHHW datum.

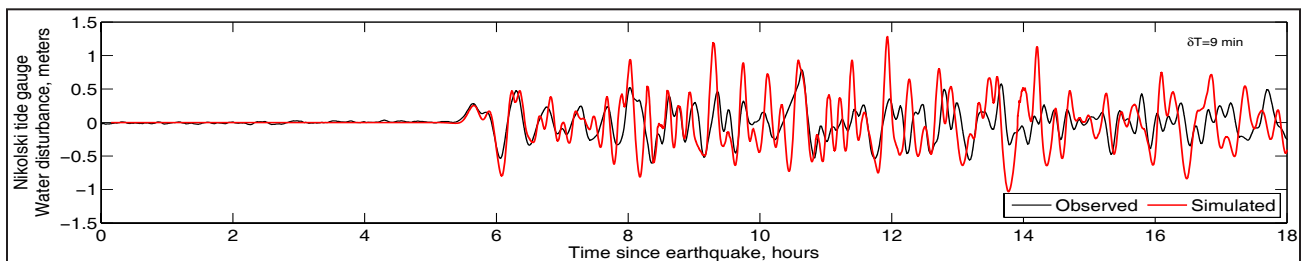


Figure 5. Comparison of modeled and observed water-level dynamics at the tide station in Nikolski during the March 11, 2011, Tohoku tsunami.

near Nikolski due to distant events is provided in the Pacific Marine Environmental Laboratory (PMEL) Tsunami Forecast Model report by Wei (in review).

The numerical modeling of the 2011 Tohoku tsunami demonstrates that the employed numerical model of tsunami propagation and runup generates tsunami waveforms that are consistent with the observed arrival times and wave phases for the first two hours after the arrival of the first wave. The later waves are higher and more dispersive. This could be due to incomplete resolution of the coastline in the Levels 1–3 grids. Overall, the model provides a good approximation of the recorded tsunami amplitudes in Mueller Cove, which indicates that the proposed coseismic deformation model adequately describes the coseismic slip distribution, and the DEM nesting is appropriate.

TSUNAMI SOURCES

It is generally thought that all of the great historic earthquakes along the Alaska–Aleutian subduction zone occurred on the megathrust—the contact surface between the subducting Pacific plate and the North American plate. Nicolsky and others (2015) provide a detailed summary of the regional plate tectonic setting, seismotectonics of the Fox Islands, and the locations of the locked and creeping zones along the Alaska–Aleutian megathrust near Umnak Island. Similar to the tsunami analyses for Unalaska and Akutan Islands (Nicolsky and others, 2015), we conducted a sensitivity study specific to the village of Nikolski and investigated waves arriving from a variety of idealized ruptures from different downdip locations in the locked region. The results of the sensitivity study are then applied to construct the maximum credible scenarios.

SENSITIVITY STUDY

To test the sensitivity of wave heights from ruptures nucleating at different downdip locations, we develop five hypothetical cases of the slip distribution (cases A–E) for M_w 8.2 earthquakes near Umnak Island (fig. 6). The relative slip distribution for all five cases is identical: uniform in the along-strike direction with tapering at the ends of the rupture and a symmetrical bell-type slip curve in the downdip direction. Between any two consecutive cases, the hypothetical rupture is offset by about 10 km (6.2 mi) in the downdip direction: Case A corresponds to a rupture patch at 50 km (31 mi) depth, Case B corresponds to a rupture patch at 40 km (25 mi) depth, and so on to Case E at 10 km (6.2 mi) depth. The along-strike location for the hypothetical ruptures is selected across Samalga Pass (between Umnak and the Islands of Four Mountains), which is a direct pathway for arrival of dangerous waves to the Bering Sea side of Umnak Island and thus to the village of Nikolski. Vertical deformation associated with each case is shown in figure 7.

There are no known geological or paleoseismological records of land-level change in this area and thus there are no constraints to calibrate the modeled ground subsidence

and uplift near the Fox Islands. In this report, we assume that all scenarios considered are geologically plausible and realistically simulate the water dynamics near the waterfront in Nikolski for each case. The simulated water levels in Mueller Cove, adjacent to Nikolski, are shown in figure 8. Note that the hypothetical earthquakes based on cases C–E produce the highest waves in Nikolski. The maximum waves for cases C–E, marked by black arrows in figure 8, arrive in two distinct 15–20 minute time intervals. Therefore, if adjacent downdip sections (corresponding to cases C and D, or to cases D and E) rupture simultaneously, the waves generated separately by each section could constructively interfere to produce a larger wave.

On the basis of the results of this downdip sensitivity study, we find that the rupture depths that have the most effect on wave height coincide with the location of rupture patches in cases C–E. We recall that the considered cases represent hypothetical M_w 8.2 earthquakes, although much larger earthquakes are possible along the Aleutian Islands (Wesson and others, 2008). As in Nicolsky and others (2015) we develop maximum credible scenarios⁵ for Nikolski as follows: we assume a maximum slip up to 35–37 m (115–121 ft) along the Fox Islands, and then attribute the maximum value of the slip around the patches which, when they rupture, result in the highest waves; the resulting waves could then constructively interfere with each other. In the instance of Nikolski, patches related to cases C–E produce the highest waves that could constructively interfere with each other. The assumed maximum slip of 35–37 m (115–121 ft) is consistent with other modeling studies (such as Butler, 2014) for this region. In the downdip direction, the slip is parameterized using the specifications of Freund and Barnett (1976), with the deeper and shallower boundaries of rupture at 5 km (3.1 mi) and 42 km (26 mi), respectively.

EARTHQUAKE SCENARIOS

Various downdip locations for the maximum slip are next considered to develop a geologically credible M_w 9.1 earthquake (scenarios 1–3) to evaluate wave arrivals and heights in Nikolski and the Pacific side of Umnak Island. Previously considered earthquakes (Nicolsky and others, 2015) with variable rupture parameters are also examined with respect to tsunami inundation at Umnak Island in scenarios 4–10.

Scenario 1: M_w 9.1 earthquake in the Fox Islands region, based on hypothetical cases C and D

This event is a hypothetical M_w 9.1 earthquake rupturing the Aleutian megathrust at the eastern part of the 1957 aftershock area. The slip is uniformly distributed in the along-strike direction of the plate interface from Unimak Island to Atka Island and is tapered on both ends of the rupture. A symmetrical bell-type slip curve, which is related to Freund and Barnett's (1976) slip skewness parameter $q = 0.5$, is assumed in the downdip direction. The maximum slip of 37 m (121 ft) is located at a depth of 25 km (16 mi), which corresponds

⁵A realistic, very complex slip distribution is not available from this modeling study. The scenarios presented attempt to capture an essence of the maximum credible scenarios and provide a starting point for development of more complex models.

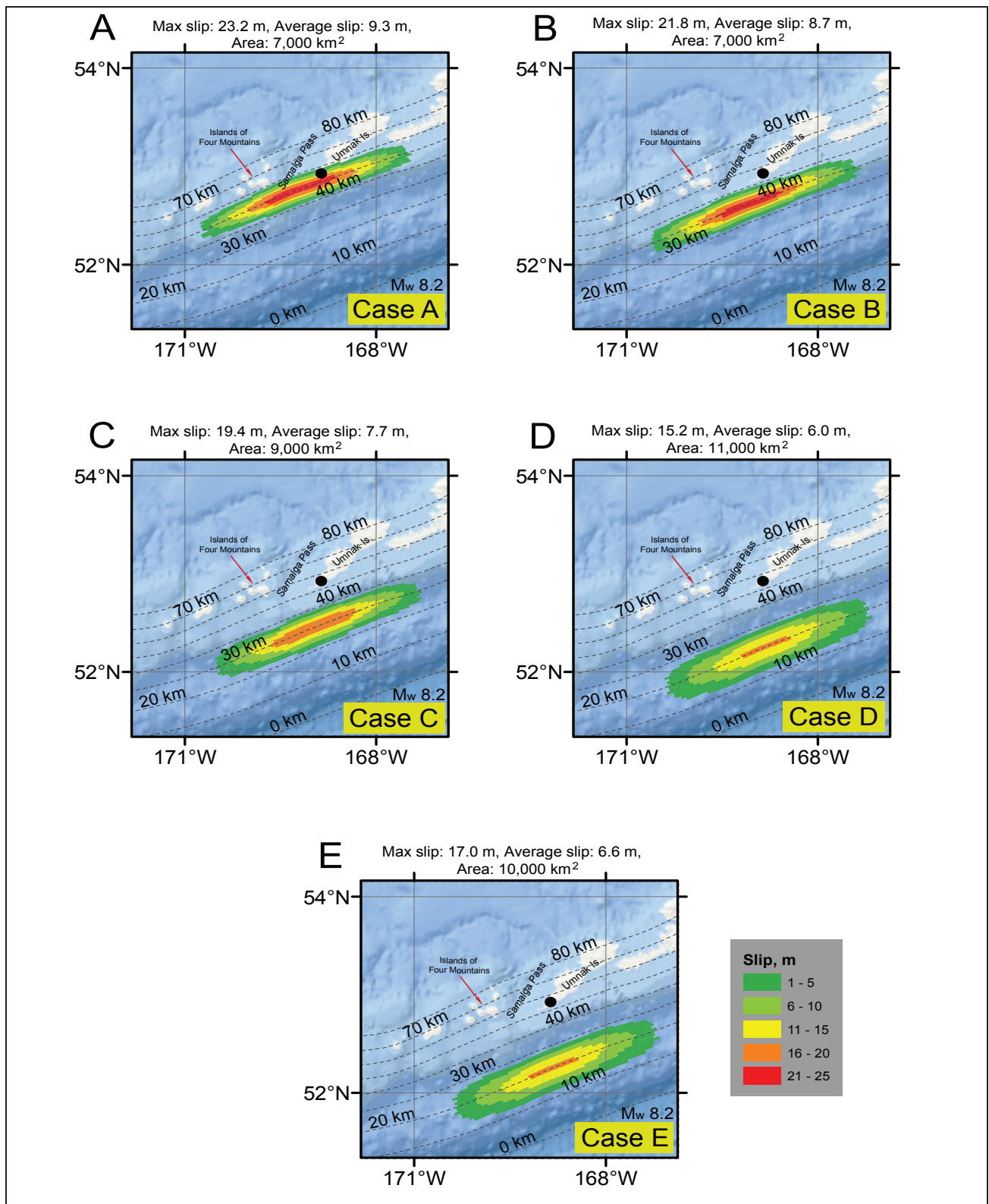


Figure 6. Assumed slip distribution along the plate interface for cases A–E, modeling a M_w 8.2 rupture across Samalga Pass. The slip location varies in the downdip direction of the plate interface while preserving the same patch configuration. Dashed lines are depth contours of the subduction interface, in kilometers. Nikolski is marked by a black circle.

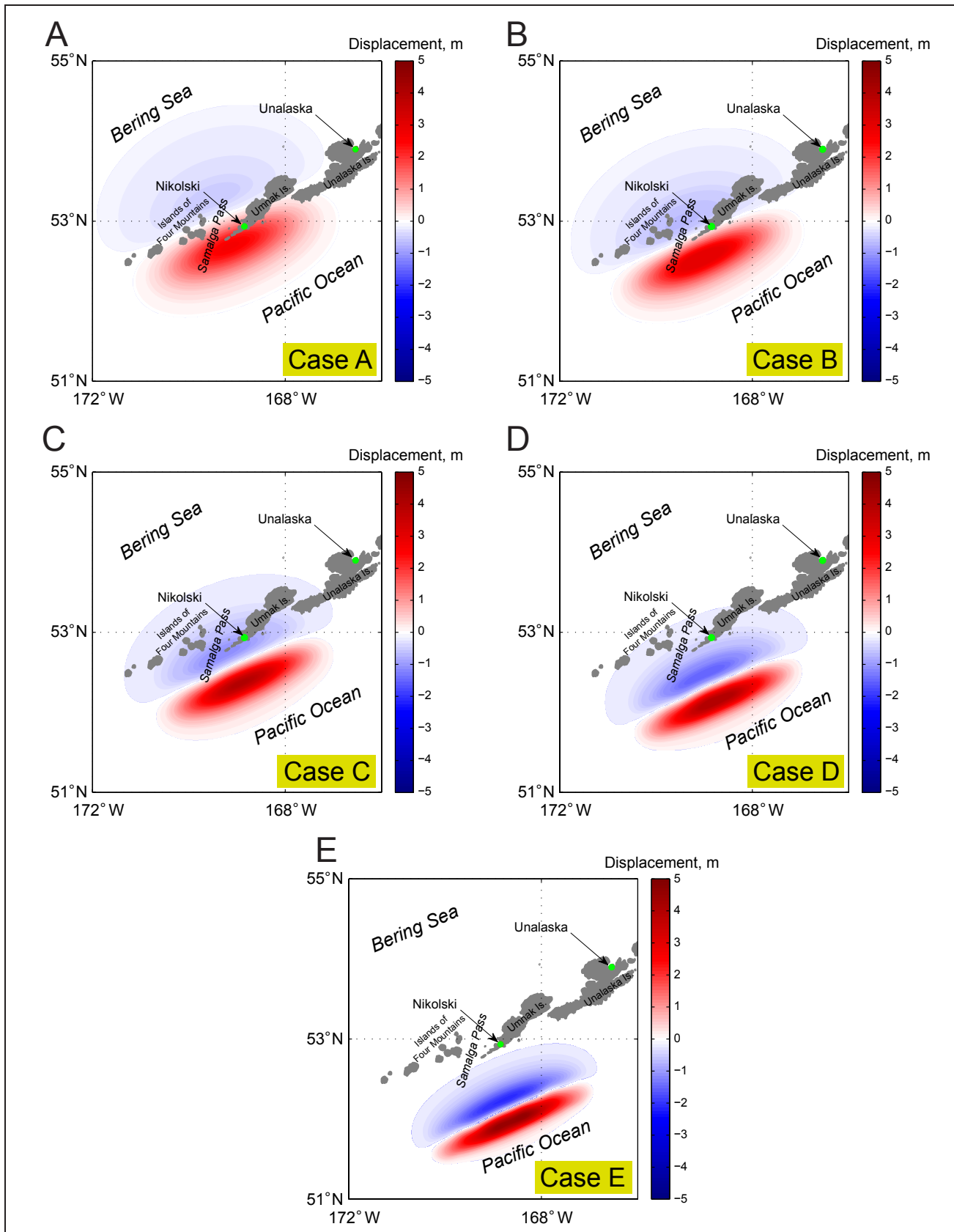


Figure 7. Computed vertical ground-surface deformation related to cases A–E (shown in fig. 6) are associated with coseismic ground subsidence; areas of uplift are shown in red.

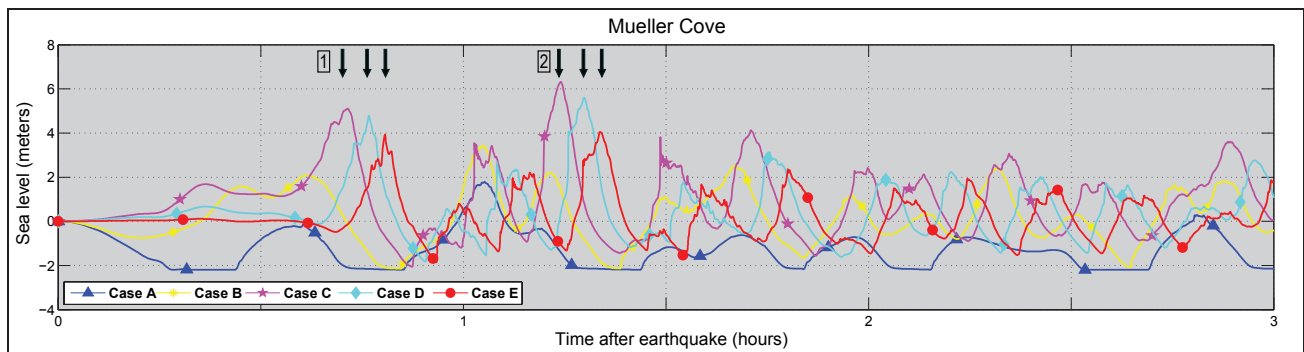


Figure 8. Modeled water-level dynamics in Mueller Cove adjacent to Nikolski for ground-surface deformations (shown in fig. 7). Black vertical arrows mark maximum waves for cases C–E, which arrive in two distinct 15–20-minute time intervals.

to a superposition of depths in cases C and D. The proposed slip distribution is shown in figure 9A; vertical coseismic deformations for this scenario are shown in figure 10A.

Although the sensitivity study indicates that scenario 1 could result in the maximum wave height in Nikolski, there are most likely other distributions of the slip (between 5 km [3.1 mi] and 42 km [26 mi] depths along the plate interface) that could result in similar maximum wave heights near the village. Therefore, to ensure that we do not accidentally omit other relevant scenarios, we supplement scenario 1 with the following two scenarios, which have a slightly skewed bell-type slip curve in the downdip direction. As in scenario 1, scenarios 2 and 3 also model a hypothetical M_w 9.1 earthquake that ruptures the Aleutian megathrust at the eastern part of the 1957 aftershock area and places a maximum slip at a different depth.

Scenario 2: M_w 9.1 earthquake in the Fox Islands region, based on hypothetical cases D and E

The slip skewness parameter, q , is set to 0.25 to model the maximum slip of 37 m (121 ft) at a depth of 15 km (9.3 mi), which corresponds to a superposition of depths in cases D and E. The proposed slip distribution is shown in figure 9B; vertical coseismic deformations for this scenario are shown in figure 10B.

Scenario 3: M_w 9.1 earthquake in the Fox Islands region, based on hypothetical case C

The slip skewness parameter, q , is set to 0.65 to model the maximum slip of 37 m (121 ft) at a depth of 30 km (19 mi), which corresponds to the location of the maximum slip in case C. The proposed slip distribution is shown in figure 9C; vertical coseismic deformations for this scenario are shown in figure 10C.

In view of the recent M_w 9.0 earthquake off the Pacific coast of Tohoku in 2011, we consider two similar events along the Aleutian megathrust. Additionally, as in Nicolsky and others (2015) we assess tsunami runup in Nikolski according to two scenarios based on the research by Butler (2014), the maximum credible scenario for Unalaska/Dutch Harbor, a hypothetical M_w 8.6 outer-rise event, and a rupture of the

Cascadia zone. Scenarios marked by an asterisk (*) are the same as in Nicolsky and others (2015).

Scenario 4: M_w 9.0 earthquake according to the SAFRR project*

This scenario is the same as scenario 4 in the Nicolsky and others (2015) tsunami modeling study for Unalaska/Dutch Harbor. The assumed slip distribution is shown in Nicolsky and others (2015, fig. 22D); the coseismic deformations for this scenario are shown in Nicolsky and others (2015, fig. 23D).

Scenario 5: M_w 9.0 SAFRR-type earthquake in the Samalga Pass region

In this scenario, we assume that the slip distribution in the downdip direction is the same as that in scenario 4, where greater slip occurs closer to the trench but is shifted westward along the trench. The slip is distributed almost uniformly along strike except for the edges of the rupture, where it tapers. The rupture is centered across Samalga Pass, between Umnak and the Islands of Four Mountains. Samalga Passage is likely the most direct pathway for arrival of dangerous waves to the Bering Sea side of Umnak Island, and hence to the village of Nikolski. The proposed slip distribution is shown in figure 9D; vertical coseismic deformations for this scenario are shown in figure 10D.

Scenario 6: M_w 9.2 East Aleutian earthquake*

This scenario is the same as scenario 7 in the Nicolsky and others (2015) tsunami modeling study for Unalaska/Dutch Harbor. The assumed slip distribution is shown in Nicolsky and others (2015, fig. 22G); vertical coseismic deformations for this scenario are shown in Nicolsky and others (2015, fig. 23G).

Scenario 7: M_w 9.25 East Aleutian earthquake*

This scenario is the same as scenario 8 in the Nicolsky and others (2015) modeling tsunami modeling study for Unalaska/Dutch Harbor. The assumed slip distribution is shown in Nicolsky and others (2015, fig. 22H); vertical coseismic deformations for this scenario are shown in Nicolsky and others (2015, fig. 23H).

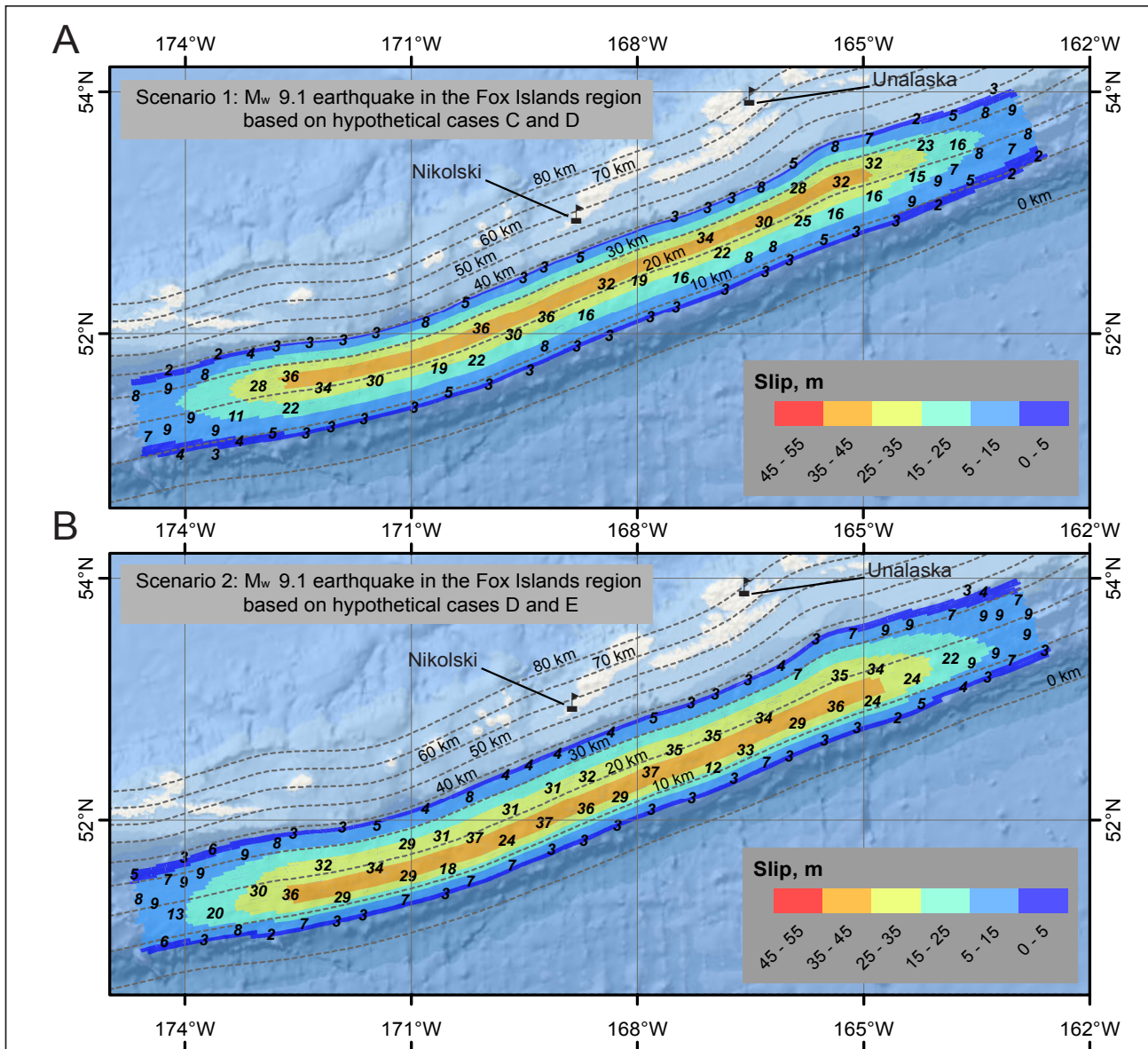


Figure 9. Proposed slip distribution along the plate interface for: (A) Scenario 1, hypothetical M_w 9.1 earthquake in the Fox Islands region, based on hypothetical cases C and D; (B) Scenario 2, hypothetical M_w 9.1 earthquake in the Fox Islands region, based on hypothetical cases D and E. The proposed slip distribution for scenarios 4, 6, 7, and 8 is depicted in Nicolisky and others (2015, figs. 22D, 22G, 22H, and 22A, respectively). Slip distributions are not provided for scenarios 9 and 10. The proposed slip distribution along the plate interface is uniform in the along-strike direction and is slightly tapered at both ends of the potential rupture. Slip values in meters are marked by small black labels. The depth contours of the Aleutian interface are shown by dashed lines.

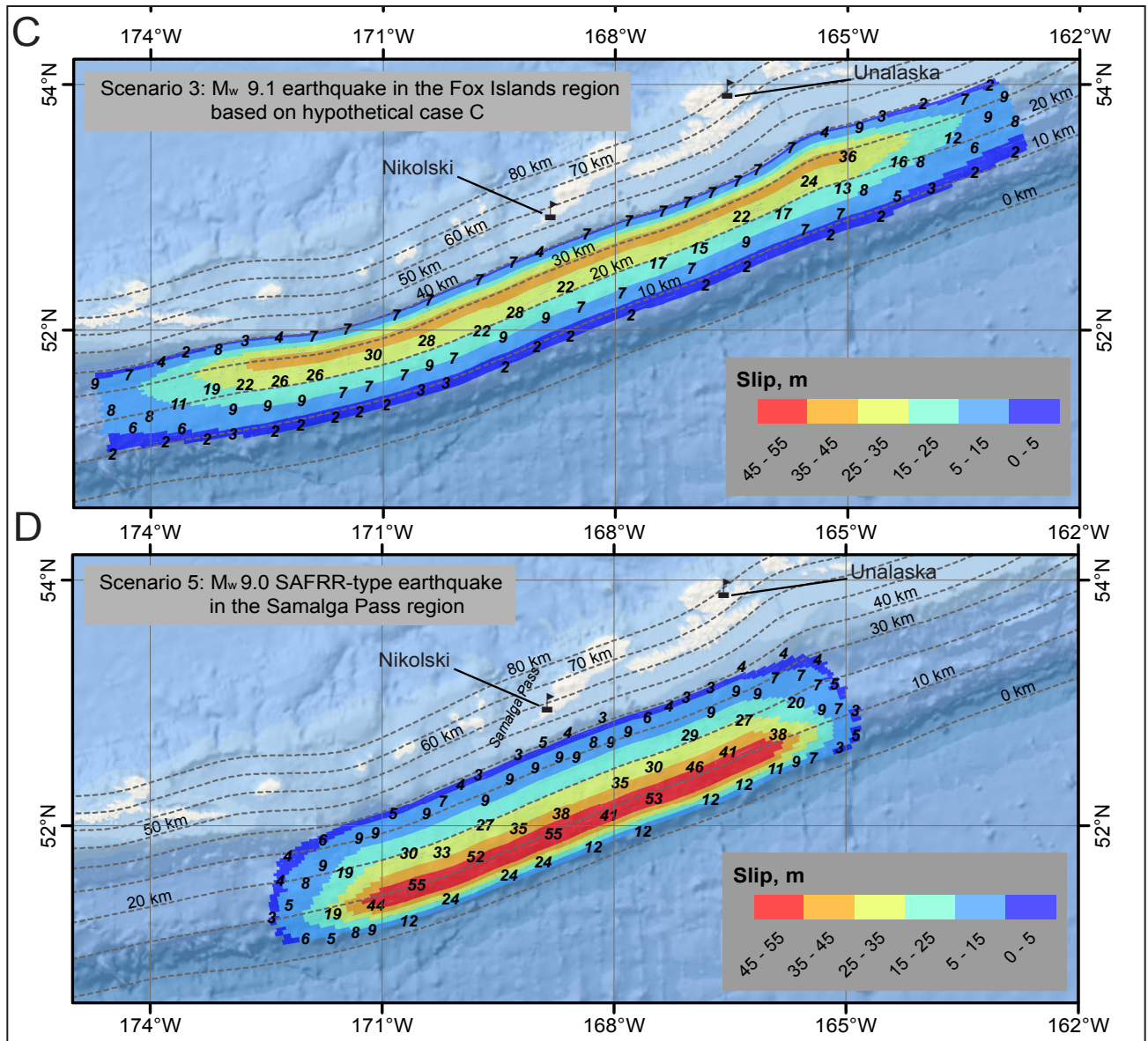


Figure 9 (continued). Proposed slip distribution along the plate interface for: (C) Scenario 3, hypothetical M_w 9.1 earthquake in the Fox Islands region, based on hypothetical case C; (D) Scenario 5, hypothetical M_w 9.0 SAFRR-type earthquake in the Samalga Pass region. The proposed slip distribution for scenarios 4, 6, 7, and 8 is depicted in Nicolosky and others (2015, figs. 22D, 22G, 22H, and 22A, respectively). Slip distributions are not provided for scenarios 9 and 10. The proposed slip distribution along the plate interface is uniform in the along-strike direction and is slightly tapered at both ends of the potential rupture. Slip values in meters are marked by small black labels. The depth contours of the Aleutian interface are shown by dashed lines.

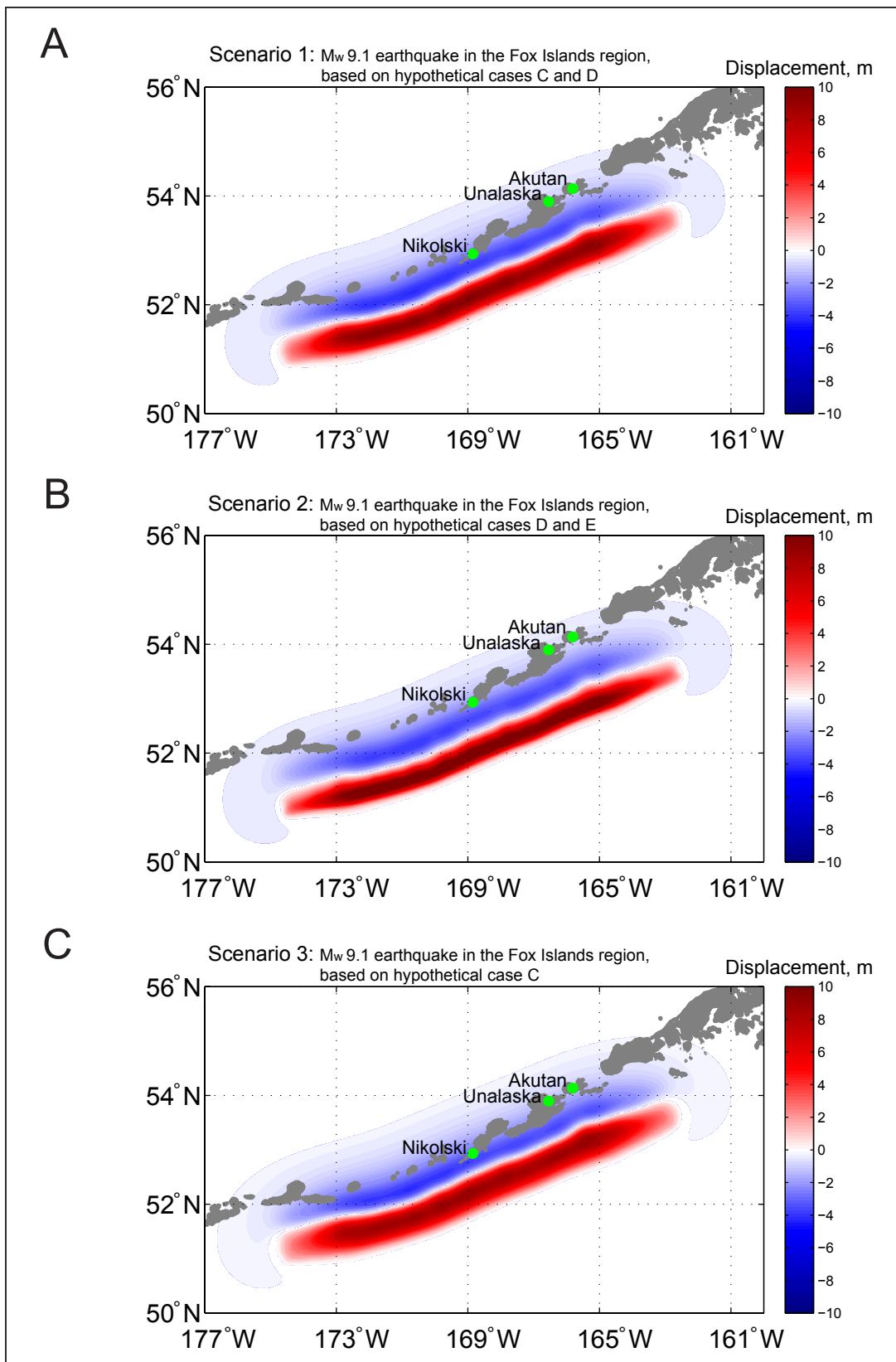


Figure 10. Computed vertical ground-surface deformation related to proposed slip distributions shown in figure 9 (fig. 10 A–D) and an outer-rise event (fig. 10E). Blue shaded areas are associated with coseismic ground subsidence; areas of uplift are shown in red.

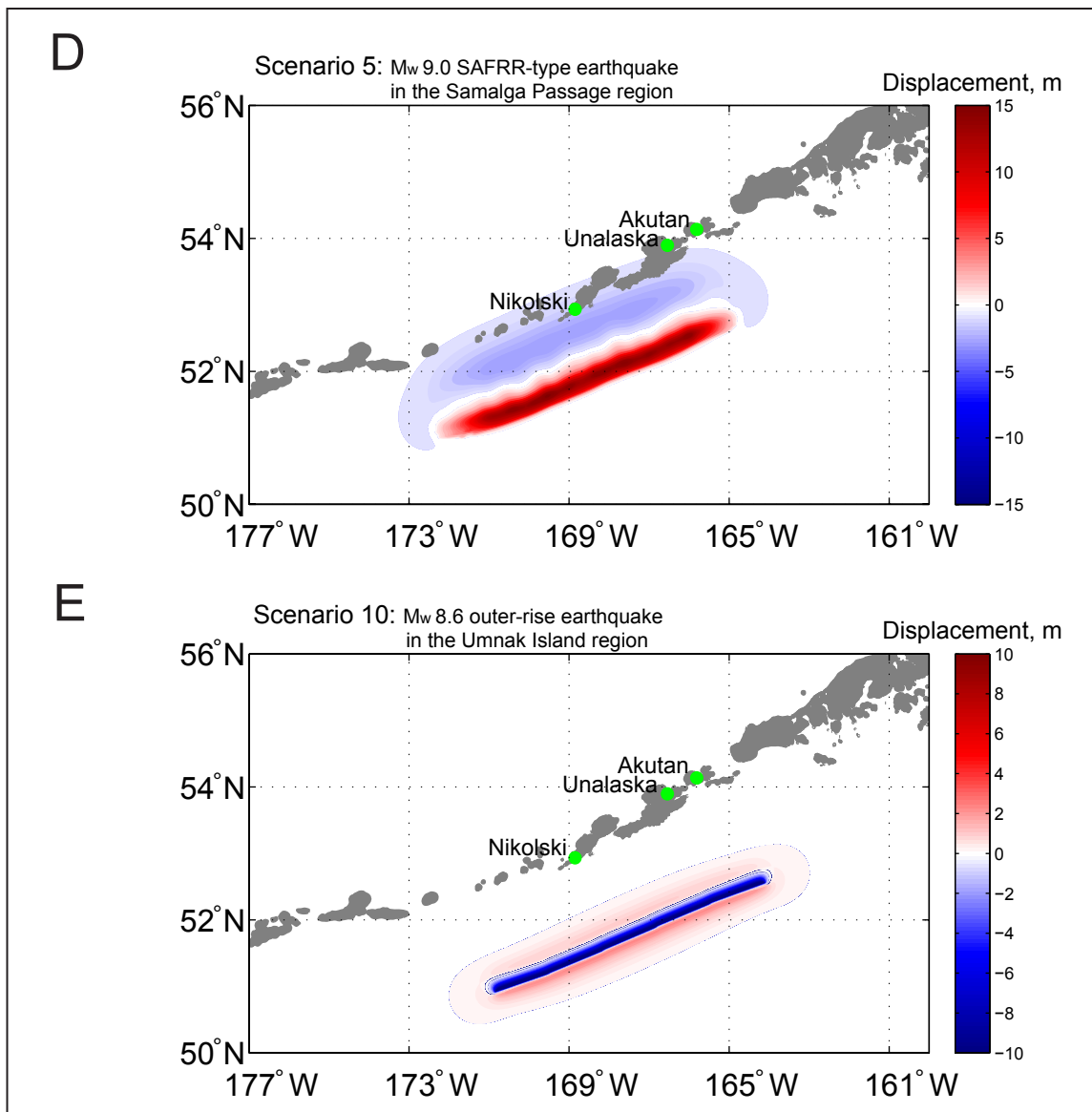


Figure 10 (continued). Computed vertical ground-surface deformation related to proposed slip distributions shown in figure 9 (fig. 10A–D) and an outer-rise event (fig. 10E). Blue shaded areas are associated with coseismic ground subsidence; areas of uplift are shown in red.

Table 2. Fault parameters for the hypothetical tensional M_w 8.6 outer-rise earthquake (scenario 10).

Latitude (°N)	Longitude (°W)	Depth (km)	Length (km)	Width (km)	Strike (deg.)	Dip (deg.)	Rake (deg.)	Slip (m)
51°31'51.6"	168°09'00.0"	2	100	15	248.18	45	-90	25
51°11'09.6"	169°29'52.8"	2	100	15	251.71	45	-90	25
52°33'14.4"	164°04'33.6"	2	100	15	250.15	45	-90	25
52°14'24.0"	165°27'36.0"	2	100	15	247.56	45	-90	25
51°53'09.6"	166°48'36.0"	2	100	15	247.42	45	-90	25

Table 3. All hypothetical scenarios used to model tsunami runup in Nikolski. Scenarios marked by an asterisk (*) indicate scenarios described in the Unalaska/Dutch Harbor modeling study by Nicolovsky and others (2015). The number of the scenario in Nicolovsky and others (2015) is stated in the parentheses after the asterisk.

Tectonic Scenarios		Depth range (km)	Maximum slip, depth range (km)	Maximum slip (m)	Maximum subsidence (m)	Maximum uplift (m)	Vertical displacement (m)	Main Street Maximum water depth (m)
1	M _w 9.1 earthquake in the Fox Islands region, based on hypothetical cases C and D	5–42	20–26	37	4.1	10.0	-2.6	14.5
2	M _w 9.1 earthquake in the Fox Islands region, based on hypothetical cases D and E	5–42	14–19	37	3.8	11.8	-1.9	13.9
3	M _w 9.1 earthquake in the Fox Islands region, based on hypothetical case C	5–42	26–31	37	3.9	9.3	-2.9	14.4
4*(4)	M _w 9.0 earthquake according to the SAFRR project	8–54	11–14	55–65	2.8	14.8	-0.0	0.0
5	M _w 9.0 SAFRR-type earthquake in the Samalga Pass region	8–54	10–12	55	2.7	15.0	-1.4	13.5
6*(7)	M _w 9.2 East Aleutian earthquake	7–50	12–18	44	4.0	14.4	-3.5	13.8
7*(8)	M _w 9.25 East Aleutian earthquake	5–31	5–18	50	4.1	21.8	-1.7	15.2
8*(1)	M _w 9.1 earthquake, Fox Islands region	8–50	40–45	37	2.9	10.8	-0.6	9.6
9*(9)	M _w 9.0–9.1 earthquake in the Cascadia subduction zone	Wang and others (2003)	Wang and others (2003)	35–45	7.5	10.9	0.0	1.1
10	M _w 8.6 outer-rise earthquake in the Umnak Island region	2–23	2–23	25	13.9	2.5	-0.1	1.2

Scenario 8: M_w 9.1 earthquake, Fox Islands region*

This scenario is the same as scenario 1 in the Nicolovsky and others (2015) tsunami modeling study for Unalaska/Dutch Harbor. The assumed slip distribution is shown in Nicolovsky and others (2015, fig. 22A); vertical coseismic deformations for this scenario are shown in Nicolovsky and others (2015, fig. 23A).

Scenario 9: M_w 9.0–9.1 earthquake in the Cascadia subduction zone*

This scenario models a rupture of the Cascadia zone, including the entire megathrust between British Columbia and northern California and is the same as scenario 9 in the Nicolovsky and others (2015) tsunami modeling study for Unalaska/Dutch Harbor. The vertical coseismic deformations for this scenario are shown in Nicolovsky and others (2015, fig. 23I).

Scenario 10: M_w 8.6 outer-rise earthquake in the Umnak Island region

We consider a hypothetical M_w 8.6 outer-rise event parallel to Umnak and Unimak islands and parameterize it by five subfaults, listed in table 2. The fault parameters required to compute seafloor deformation are the epicenter location, area, dip, rake, strike, and amount of slip on the fault. We use the equations of Okada (1985) to calculate distribution of coseismic uplift and subsidence resulting from this slip distribution. The dip of each subfault is in a range reported

by Stauder (1968), and we assume that the hypothetical earthquake ruptures through the entire slab. Vertical coseismic deformations for this scenario are shown in figure 10E.

MODELING RESULTS

We performed numerical calculations for each of the ten hypothetical earthquake scenarios. The water dynamics are modeled in each grid (listed in table 1) and we compute the extent of inundation only in the high-resolution grids. The simulated extents of inundation in Nikolski for all considered scenarios are shown in figure 11 and wave heights are listed for 22 locations around Nikolski in Table A-1.

We begin discussion of the modeling results by noting that scenario 1 (a hypothetical M_w 9.1 earthquake) predicts a 16 m (52.5 ft) wave at the computational station in Mueller Cove. Scenarios 2 and 3 display similar waves of about 15–16 m (49.2–52.5 ft) at the same station. The modeled water-level dynamics for scenarios 1–3 in the first four hours after the earthquake are plotted in figure 12A. As noted earlier, the Bering Sea side of the island is thought to be rather protected from tsunamis. This hypothesis is somewhat supported by numerical modeling of water dynamics along the Pacific side of Umnak Island. The numerical experiments demonstrate that, according to scenarios 1–3, water waves along the Pacific side could reach a height of 42 m (138 ft) above sea level, as illustrated in figure 13A. The prediction

of high waves on the Pacific side of Umnak Island is also supported by the presence of drift logs at 23 m (75.4 ft) above sea level (Witter and others, 2014). The numerical simulations reveal that the first wave could arrive at Nikolski within 20 minutes after the earthquake, whereas the highest wave could arrive 40 minutes after the earthquake. Significant wave activity could continue for at least 4 hours after the earthquake, with waves reaching 12 m (39.4 ft) above the pre-earthquake sea level. The water-level fluctuations gradually reduce after 4 hours but continue to be dangerously high for at least 18 hours after the earthquake.

Scenario 4, a hypothetical Tohoku-type earthquake (considered in the SAFRR project) between Shumagin and Kodiak islands, produces a 1 m (3.3 ft) wave in Mueller Cove. The modeled water level is shown by the blue line in figure 12B. The hypothetical tsunami might flood only low-lying areas along the shoreline. However, scenario 5, which simulates the SAFRR-type earthquake just offshore of Umnak Island, results in 15 m (49.2 ft) waves in Mueller Cove and produces significant inundation of the village. The estimated extent of inundation as well as the water-level dynamics are shown in figures 10D and 12C, respectively. On the Pacific side of the island, scenario 5 could result in a 55 m (180.4 ft) wave, as shown in figure 13C. During the 2011 Tohoku event, the local runup reached 35–40 m (115–131 ft) (EERI/ERI/ITST, 2011) and was comparable to the numerical results. Waves from scenario 5 might overtop the coastal banks on the Pacific side of Umnak Island and then continue downhill to flood Umnak Lake.

The modeled inundation for scenarios 6 and 7 resembles the inundation simulated by scenario 5. In the computational experiment, the 15–17 m (49.2–55.8 ft) waves flood the city and penetrate deep beyond Umnak Lake. Inundation for scenario 7 floods the entire village and parts of the landing strip and represents the worst-case scenario for the village. The modeled water-level dynamics near the village and on the Pacific side of the island for these two scenarios are shown in figures 12C and 13C, respectively.

Scenario 8, which results in a devastating tsunami in Unalaska/Dutch Harbor, also produces a significant tsunami in Nikolski. Although the simulated runup from scenario 8 is less than that generated by scenarios 1–3 and 5–7, it still significantly inundates the village and Umnak Lake. The water-level dynamics in Mueller Cove and on the Pacific side for scenario 8 are shown in figures 12C and 13C, respectively.

Scenarios 9 and 10 could produce flooding in low-lying areas as depicted in figure 11, and a series of erratic waves could cause dangerous currents in Mueller Cove. Significant wave action could continue afterward for at least 8 hours.

TIME SERIES

To help emergency managers assess the tsunami hazard in Nikolski we supplement the inundation map with the time series of the modeled water level and velocity dynamics at certain locations around the community (appendix A). For each labeled location in figure A-1, we plot the sea level

and water velocity in figures A-2 and A-3, respectively. Zero time corresponds to the time when the earthquake occurs. The pre-earthquake elevation/depth with respect to the MHHW is stated for each location. The post-earthquake elevations/depth corresponding to the MHHW datum are also listed for each scenario. To show the height of arriving tsunamis for offshore locations we use a vertical datum with a zero mark corresponding to the pre-earthquake sea level. The dashed lines show water levels after the tsunami. The velocity magnitude is calculated as water flux divided by water depth, thus the velocity value can have large uncertainties when the water depth is small. In the plots provided, the velocity is computed only where the water depth is greater than 0.3 m (1 ft).

Analysis of the time series plot shows that a hypothetical earthquake with a magnitude of 9.0 can cause devastating waves that inundate the entire village and cause flooding beyond Umnak Lake. The maximum water depth and velocity for the all considered scenarios are listed in table A-1. The numerical modeling predicts that tsunami currents in Mueller Cove could reach a velocity of 8.1 m/s (15.7 kt).

SOURCES OF ERRORS AND UNCERTAINTIES

The hydrodynamic model used to calculate propagation and runup of tsunami waves is a nonlinear, flux-formulated, shallow-water model (Nicolosky and others, 2011b) that has passed the validation and verification tests required for models used in production of tsunami inundation maps (Synolakis and others, 2007; NTHMP, 2012). Details about the limitations of the employed modeling approach are described in the earlier reports by Suleimani and others, (2010; 2013; 2015) and Nicolosky and others (2011a, 2011b, 2013, 2014; 2015) as well as in NTHMP (2012).

SUMMARY

We present the results of numerical modeling of earthquake-generated tsunamis for Nikolski, Alaska. Numerical predictions of the tsunami height and current velocities for all considered scenarios are provided in Table A-1. The earthquake scenarios considered in this report are in the range of magnitude 8.0 through 9.2 for the Western Aleutian segment in the USGS Probabilistic Seismic Hazard Assessment for Alaska (Wesson and others, 2007, 2008). Hypothetical scenarios 1–3 and 5–7 ($M_w > 9.0$ earthquakes, along the Fox Islands region of the subduction zone) result in the “worst case” tsunami-inundation hazards for Nikolski. Each of these considered scenarios predicts a devastating tsunami that could crush the village as a series of waves in a continuing motion for more than 4 hours after the earthquake.

We emphasize that each of the scenarios considered are geologically reasonable and present potential hazards to the community. The map in sheet 1, showing the results of our modeling for Nikolski, has been completed using the best information available and is believed to be accurate; however, its preparation required many assumptions. We considered a suite of tectonic scenarios and provide an estimate of

maximum credible tsunami inundation for each scenario. Actual conditions during a tsunami event could vary from those considered, so the accuracy cannot be guaranteed. The limits of inundation shown should be used only as a guideline for emergency planning and response action. Actual areas inundated will depend on specifics of the earth deformation, land construction, and tide level, and might differ from areas shown on the map. The information on this map is intended to assist state and local agencies in planning emergency evacuation and tsunami response actions in the event of a major tsunamigenic earthquake. These results are not intended for land-use regulation or building-code development.

ACKNOWLEDGMENTS

This project received support from the National Oceanic and Atmospheric Administration (NOAA) under Reimbursable Service Agreements ADN 942017 and 952011 with the State of Alaska's Division of Homeland Security and Emergency Management (a division of the Department of Military and Veterans Affairs). Numerical calculations for this work were supported by a grant of High Performance Computing (HPC) resources from the Arctic Region Supercomputing Center (ARSC) at the University of Alaska Fairbanks. A thoughtful review by De Anne Stevens improved the report.

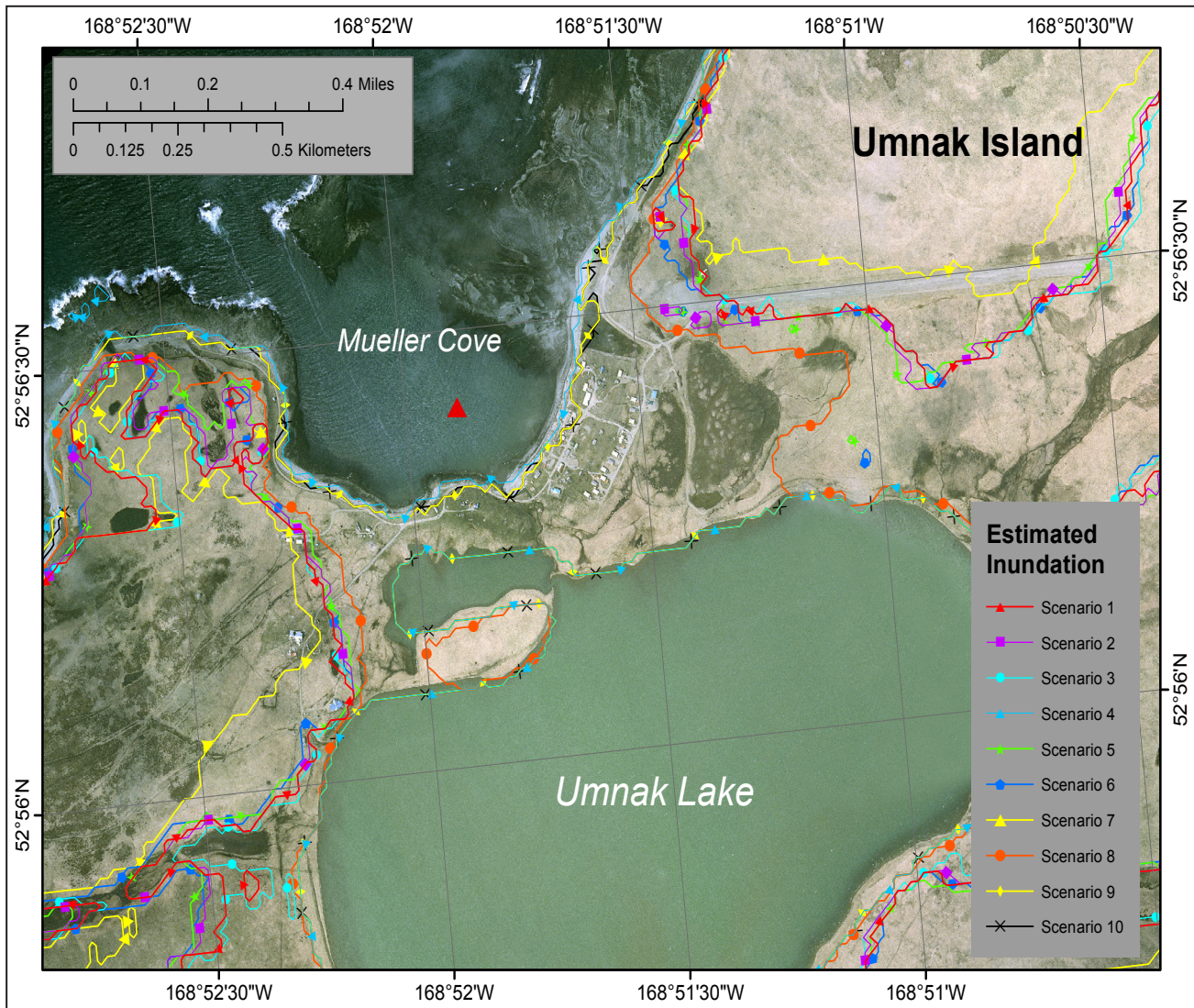


Figure 11. Modeled potential inundation in Nikolski by tectonic waves for all scenarios. Due to the steep topography, inundation areas for several tsunami scenarios have a common boundary and the plotted extents of the inundation areas overlie each other in places. The location with the recorded water-level dynamics in Mueller Bay is marked by the red triangle.

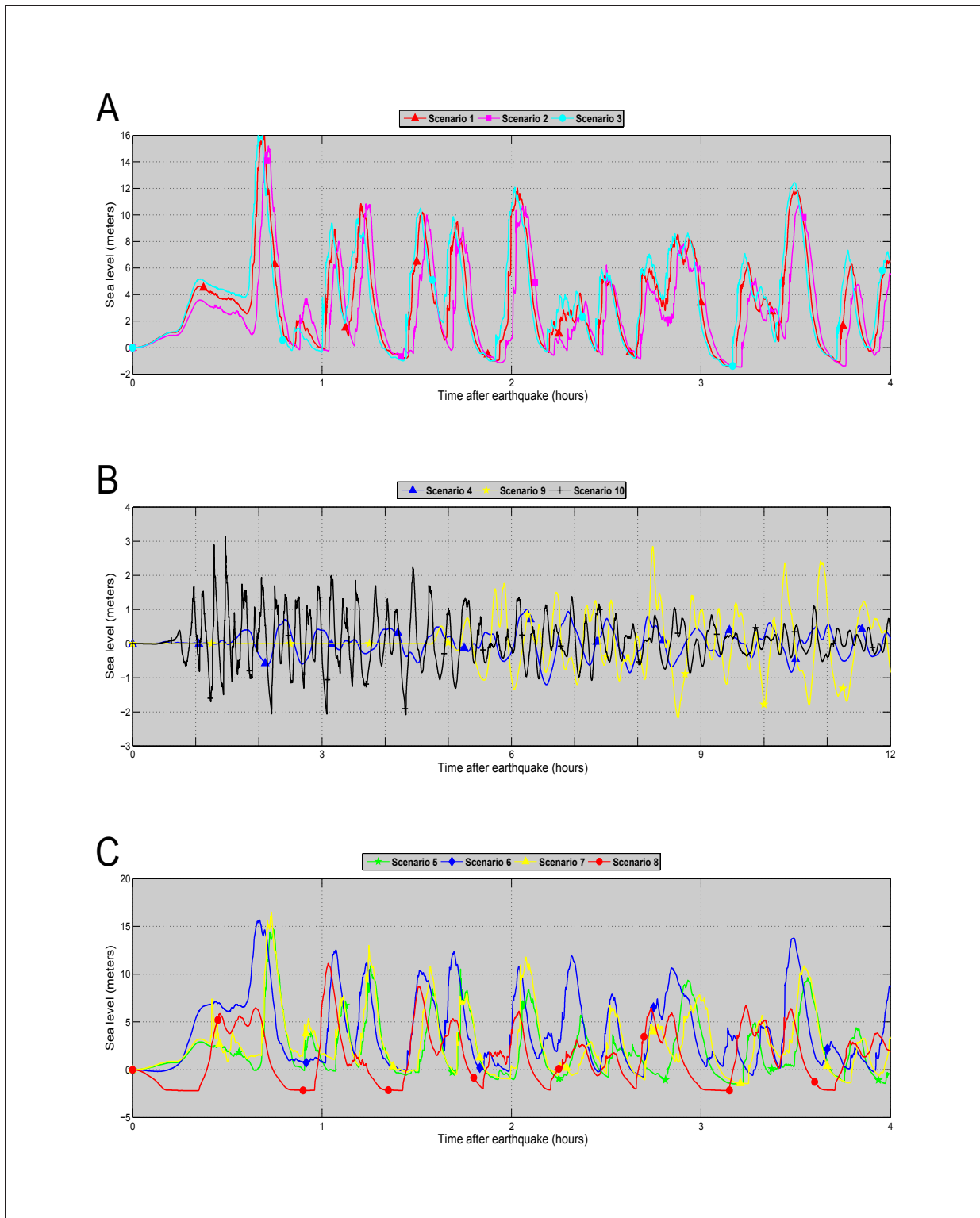


Figure 12. Modeled time series of water level in Mueller Cove: (A) for scenarios 1–3; (B) for scenarios 4, 9, and 10; and (C) for scenarios 5–8. The station location is marked by the red triangle in figure 11. The vertical datum is such that zero corresponds to the pre-earthquake sea level.

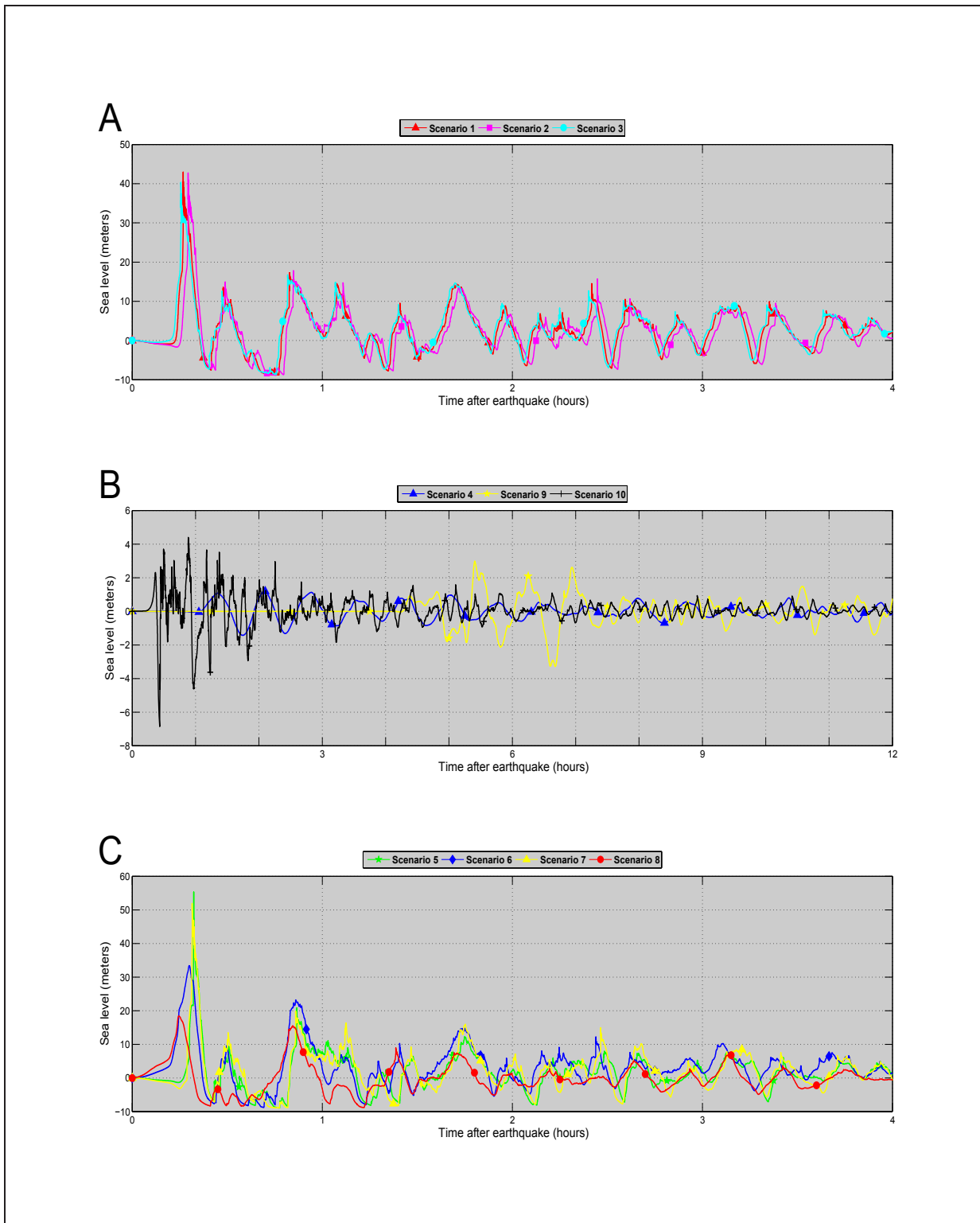


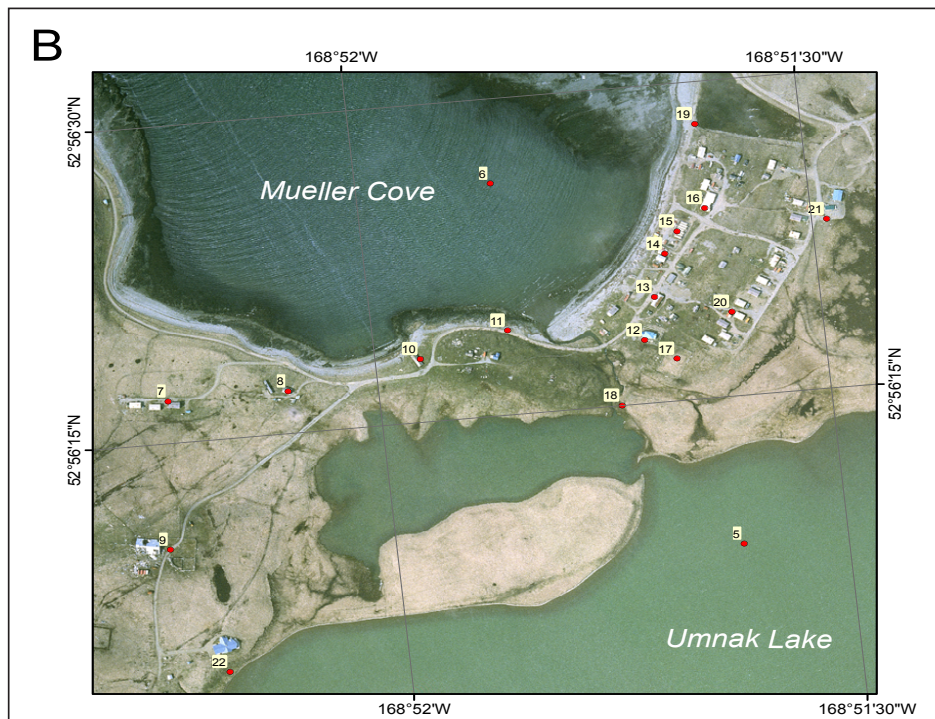
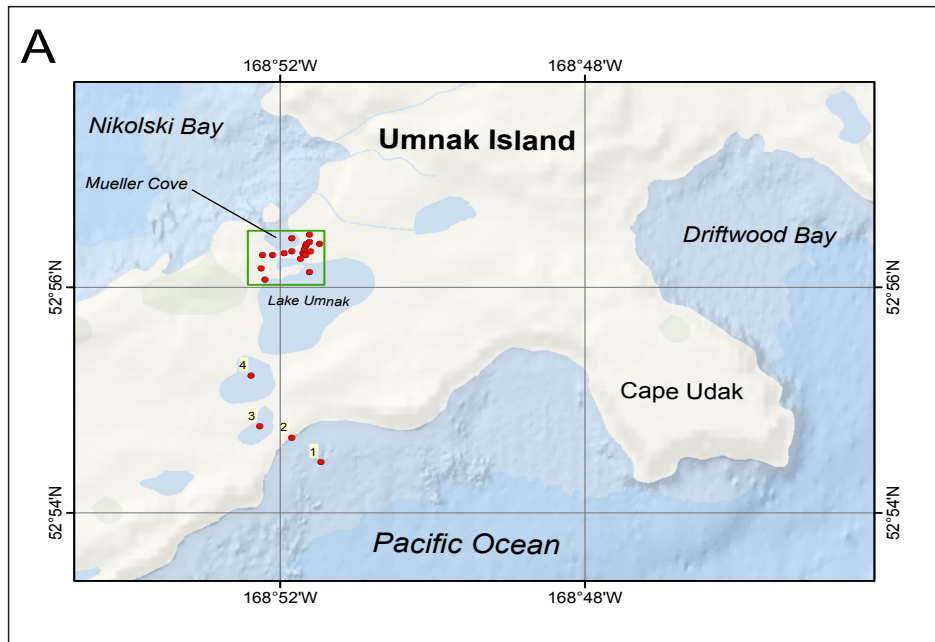
Figure 13. Modeled time series of water level along the Pacific coast of Umnak Island: (A) for scenarios 1–3; (B) for scenarios 4, 9, and 10; and (C) for scenarios 5–8. The station location is marked by the green triangle in figure 2A. The vertical datum is such that zero corresponds to the pre-earthquake sea level.

REFERENCES

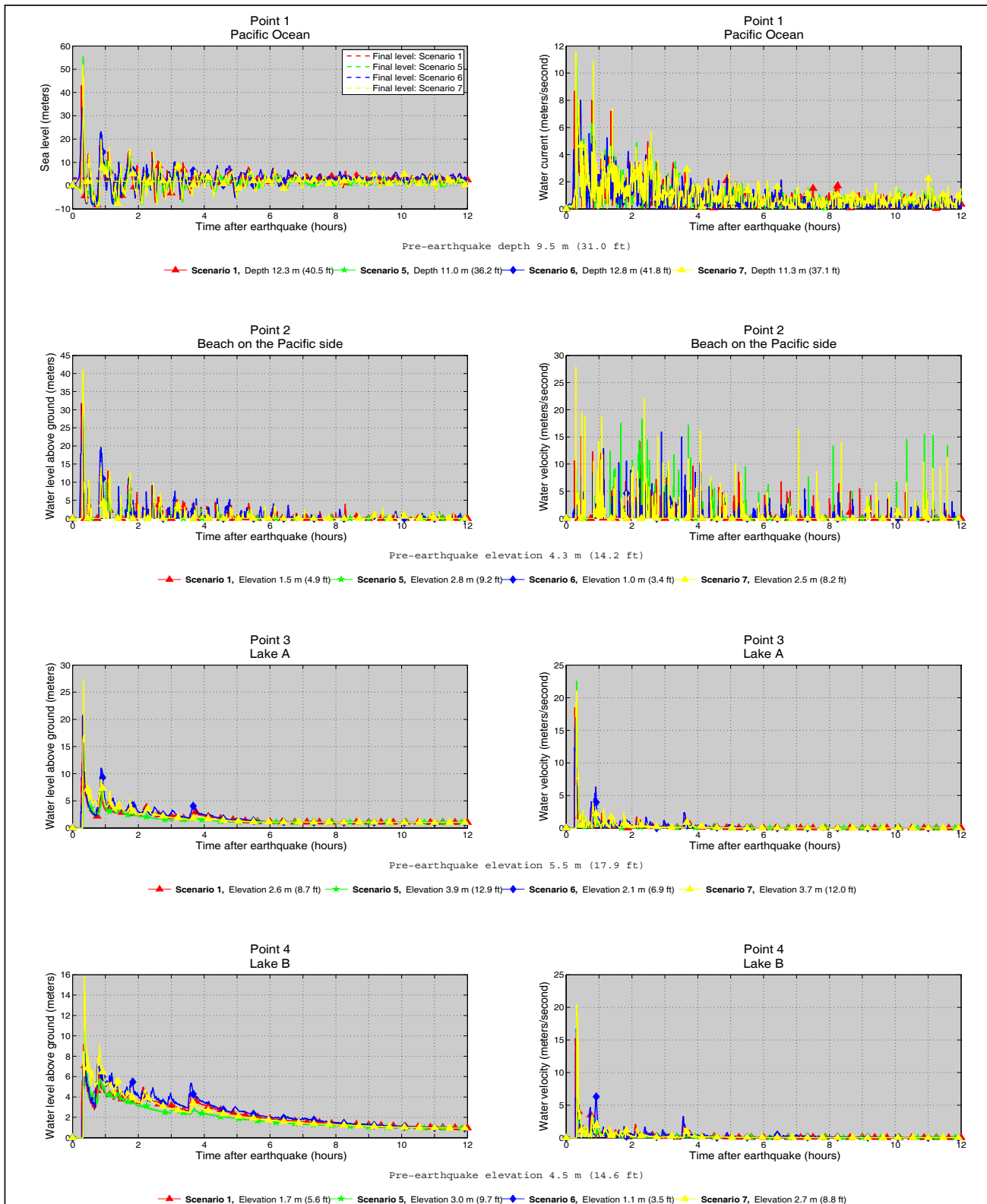
- Alaska Earthquake Center, 2015, Alaska Earthquake Center online catalog: University of Alaska Geophysical Institute. http://www.aeic.alaska.edu/html_docs/db2catalog.html (last accessed 11-25-15).
- Aigner, J.S., 1974, Studies in the early prehistory of Nikolski Bay, 1937–1971: Fairbanks, University of Alaska Fairbanks Rasmuson Library, Anthropological Papers of the University of Alaska, v. 16, no. 1, p. 9–25.
- Aigner, J.S., 1976, Dating the early Holocene maritime village of Anangula: Fairbanks, University of Alaska Fairbanks Rasmuson Library, Anthropological Papers of the University of Alaska, v. 18, p. 51–62.
- Aleutian Pribilof Island Association, 2015, “Nikolski” [website], <http://www.apiai.org/tribes/nikolski/> (last accessed 6/9/2015).
- Beasley, L., McLean, S.J., Eakins, B.W., Carignan, K.S., Love, M.R., and Sutherland, M., 2014, Digital elevation models of Nikolski, Alaska—Procedures, data sources, and analysis, prepared for the National Tsunami Hazard Mitigation Program (NTHMP) and the University of Alaska Fairbanks (UAF): Boulder, CO, NOAA National Geophysical Data Center (NGDC), Boulder, Colorado.
- Boyd, T.M., and Nabelek, J.L., 1988, Rupture process of the Andreanof Islands earthquake of May 7, 1986: Bulletin of the Seismological Society of America, v. 78, no. 5, p. 1,653–1,673.
- Butler, Rhett, 2014, Great Aleutian tsunamis: Honolulu, Hawai’i Institute of Geophysics and Planetology, Peer-Reviewed Report HIGP-2014-1, 170 p. Available from <http://www.higp.hawaii.edu/reports/2014/>.
- Carver, G.A., and Plafker, George, 2008, Paleoseismicity and neotectonics of the Aleutian subduction zone—An overview, in Freymueller, J.T., Haeussler, P.J., Wesson, R.L., and Ekström, G., eds., Active Tectonics and Seismic Potential of Alaska: American Geophysical Union Geophysical Monograph 179, p. 43–63.
- DCCED/DCRA (Alaska Department of Commerce, Community, and Economic Development, Division of Community & Regional Affairs), 2013, “Community Database Online: Nikolski” [website], <http://commerce.alaska.gov/cra/DCRAExternal/community/Details/e569dafaa01c-4f00-92c2-b27d9ee32ea8> (last accessed 6/9/2015).
- Dunbar, P.K., and Weaver, C.S., 2008, U.S. states and territories national tsunami hazard assessment—Historical record and sources for waves: National Oceanic and Atmospheric Administration and U.S. Geological Survey, Technical Report, 59 p. http://nthmp.tsunami.gov/documents/Tsunami_Assessment_Final.pdf
- EERI (Earthquake Engineering Research Institute), ERI (Earthquake Research Institute Japan), and ITST (International Tsunami Survey Teams), 2011, Learning From Earthquakes—The Japan Tohoku tsunami of March 11, 2011: EERI Earthquake Clearinghouse, EERI Special Earthquake Report Series—Learning from Earthquakes, 15 p. www.eqclearinghouse.org/2011-03-11-sendai/files/2011/11/Japan-eq-report-tsunami2.pdf
- Freund, L.B., and Barnett, D.M., 1976, A two-dimensional analysis of surface deformation due to dip-slip faulting: Bulletin of the Seismological Society of America, v. 66, p. 667–675.
- Lander, J.F., 1996, Tsunamis affecting Alaska, 1737–1996: Boulder, CO, National Oceanic and Atmospheric Administration, National Geophysical Data Center (NGDC), Key to Geophysical Research Documentation, v. 31, 155 p.
- Leica Geosystems AG, 2002, GPS User Manual, Version 4, Leica Geosystems AG, Heerbrugg, Switzerland, 62 p.
- Lim, E., Taylor, L.A., Eakins, B.W., Carignan, K.S., Caldwell, R.J., Grothe, P.R., and Friday, D.Z., 2011, Digital Elevation Model of Nikolski, Alaska: Procedures, Data Sources and Analysis, NOAA Technical Memorandum NESDIS NGDC-47, U.S. Dept. of Commerce, Boulder, CO, 24 p. <http://www.ngdc.noaa.gov/dem/squareCellGrid/download/590>
- McCartney, A.P., and Turner, II, C.G., 1966, Stratigraphy of the Anangula unifacial core and blade site: Arctic Anthropology, v. 3, no. 2, p. 28–40.
- National Geophysical Data Center/World Data Service (NGDC/WDS), in progress, Global historical tsunami database at NGDC, 2100 BC to present (interactive map): National Geophysical Data Center, NOAA, <https://www.commerce.alaska.gov/dcr/DCRAExternal/community/Details/06afc3d9-b26d-407e-8c0a-791dee3d79eb>
- National Tsunami Hazard Mapping Program (NTHMP), 2010, Guidelines and best practices for tsunami inundation modeling for evacuation planning: National Oceanic and Atmospheric Administration (NOAA), NTHMP Mapping & Modeling Subcommittee.
- National Tsunami Hazard Mapping Program (NTHMP), 2012, Proceedings and results of the 2011 NTHMP Model Benchmarking Workshop: Boulder, CO, U.S. Department of Commerce/NOAA/NTHMP, NOAA Special Report, 436 p. <http://nthmp.tsunami.gov>
- Nicolosky, D.J., Suleimani, E.N., Combellick, R.A., and Hansen, R.A., 2011a, Tsunami inundation maps of Whittier and western Passage Canal, Alaska: Alaska Division of Geological & Geophysical Surveys Report of Investigation 2011-7, 65 p. <http://dx.doi.org/10.14509/23244>
- Nicolosky, D.J., Suleimani, E.N., Freymueller, J.T., and Koehler, R.D., 2015, Tsunami inundation maps of Fox Islands communities, including Dutch Harbor and Akutan, Alaska: Alaska Division of Geological & Geophysical Surveys Report of Investigation 2015-5, 67 p., 2 sheets, scale 1:12,500. <http://dx.doi.org/10.14509/29414>
- Nicolosky, D.J., Suleimani, E.N., Haeussler, P.J., Ryan, H.F.,

- Koehler, R.D., Combellick, R.A., and Hansen, R.A., 2013, Tsunami inundation maps of Port Valdez, Alaska: Alaska Division of Geological & Geophysical Surveys Report of Investigation 2013-1, 77 p., 1 sheet, scale 1:12,500. <http://dx.doi.org/10.14509/25055>
- Nicolsky, D.J., Suleimani, E.N., and Hansen, R.A., 2011b, Validation and verification of a numerical model for tsunami propagation and runup: *Pure and Applied Geophysics*, v. 168, p. 1,199–1,222. <http://dx.doi.org/10.1007/s00024-010-0231-9>
- Nicolsky, D.J., Suleimani, E.N., and Koehler, R.D., 2014, Tsunami inundation maps of Cordova and Tatitlek, Alaska: Alaska Division of Geological & Geophysical Surveys Report of Investigation 2014-1, 49 p. <http://dx.doi.org/10.14509/27241>
- Okada, Yoshimitsu, 1985, Surface deformation due to shear and tensile faults in a half-space: *Bulletin of the Seismological Society of America*, v. 75, no. 4, p. 1,135–1,154.
- Stauder, William, 1968, Mechanism of the Rat Island earthquake sequence of February 4, 1965, with relation to island arcs and sea floor spreading: *Journal of Geophysical Research*, v. 73, no. 12 p. 3,847–3,858.
- Suleimani, E.N., Nicolsky, D.J., West, D.A., Combellick, R.A., and Hansen, R.A., 2010, Tsunami inundation maps of Seward and northern Resurrection Bay, Alaska: Alaska Division of Geological & Geophysical Surveys Report of Investigation 2010-1, 47 p., 3 sheets, scale 1:12,500. <http://dx.doi.org/10.14509/21001>
- Suleimani, E.N., Nicolsky, D.J., and Koehler, R.D., 2013, Tsunami inundation maps of Sitka, Alaska: Alaska Division of Geological & Geophysical Surveys Report of Investigation 2013-3, 76 p., 1 sheet, scale 1:250,000. <http://dx.doi.org/10.14509/26671>
- Suleimani, E.N., Nicolsky, D.J., and Koehler, R.D., 2015, Tsunami inundation maps of Elfin Cove, Gustavus, and Hoonah, Alaska: Alaska Division of Geological & Geophysical Surveys Report of Investigation 2015-1, 79 p. <http://dx.doi.org/10.14509/29404>
- Synolakis, C.E., Bernard, E.N., Titov, V.V., Kânoğlu, U., and González, F.I., 2007, Standards, criteria, and procedures for NOAA evaluation of tsunami numerical models: Seattle, NOAA/Pacific Marine Environmental Laboratory, Technical Memorandum OAR PMEL-135, 55 p.
- Tang, Liujian, Titov, V.V., Bernard, E.N., Wei, Yong, Chamberlain, C.D., Newman, J.C., Mofjeld, H.O., Arcas, Diego, Eble, M.C., Moore, Christopher, Uslu, Burak, Pells, Clint, Spillane, Michael, Wright, Lindsey, and Gica, Edison, 2012, Direct energy estimation of the 2011 Japan tsunami using deep-ocean pressure measurements: *Journal of Geophysical Research—Oceans*, v. 117, no. C8, p. 8. <http://dx.doi.org/10.1029/2011JC007635>
- Wei, Yong, in review, PMEL tsunami forecast model—Development of a tsunami forecast model for Nikolski, Alaska: NOAA/Pacific Marine Environmental Laboratory.
- Wesson, R.L., Boyd, O.S., Mueller, C.S., Bufe, C.G., Frankel, A.D., and Petersen, M.D., 2007, Revision of time-independent probabilistic seismic hazard maps for Alaska: U.S. Geological Survey Open-File Report 2007-1043, 33 p.
- Wesson, R.L., Boyd, O.S., Mueller, C.S., and Frankel, A.D., 2008, Challenges in making a seismic hazard map for Alaska and the Aleutians, in Freymueller, J.T., Haeussler, P.J., Wesson, R., and Ekström, G., eds., *Active Tectonics and Seismic Potential of Alaska*: Washington, D.C., American Geophysical Union, Geophysical Monograph v. 179, p. 385–397.
- William, L.S., and Marsh, Gordon, 1951, A new view of the history of the Aleutians: *Arctic*, v. 4, no. 2, p. 75–88.
- Witter, R.C., Briggs, R.W., Koehler, R.D., Gelfenbaum, G., Engelhart, S., Nelson, A., Carver, G., Bender, A., and Hemphill-Haley, E., 2014, Evidence for high tsunamis in the Fox Islands implies repeated Aleutian megathrust earthquakes in the Unalaska seismic gap: *Seismological Society of America, Annual meeting, Anchorage, AK*, April 30–May 2, 2014.

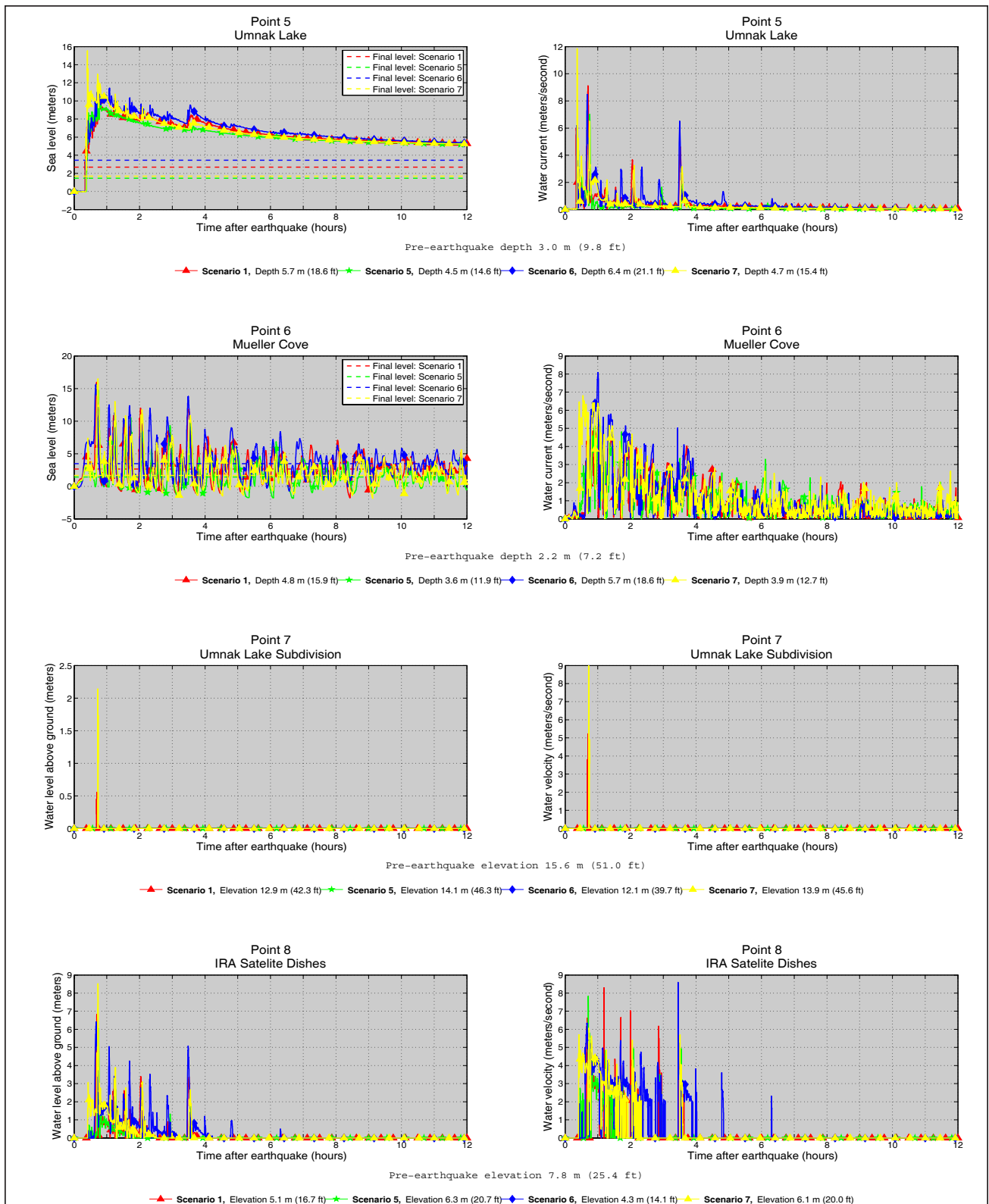
APPENDIX A



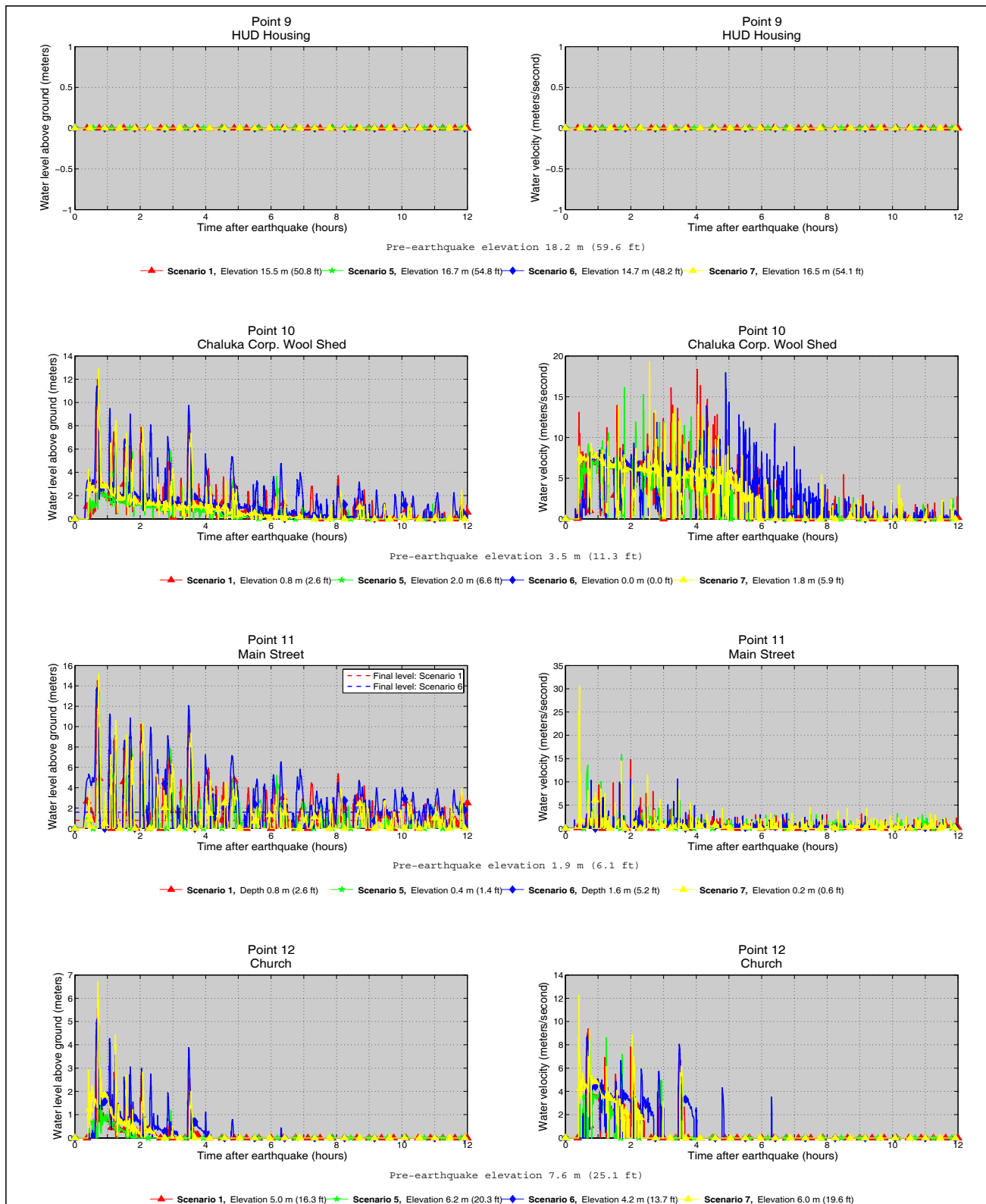
Appendix A-1. Locations of time series points on western Umnak Island (A) and in the village of Nikolski (B). The longitude and latitude locations of the time series points are listed in table A-1.



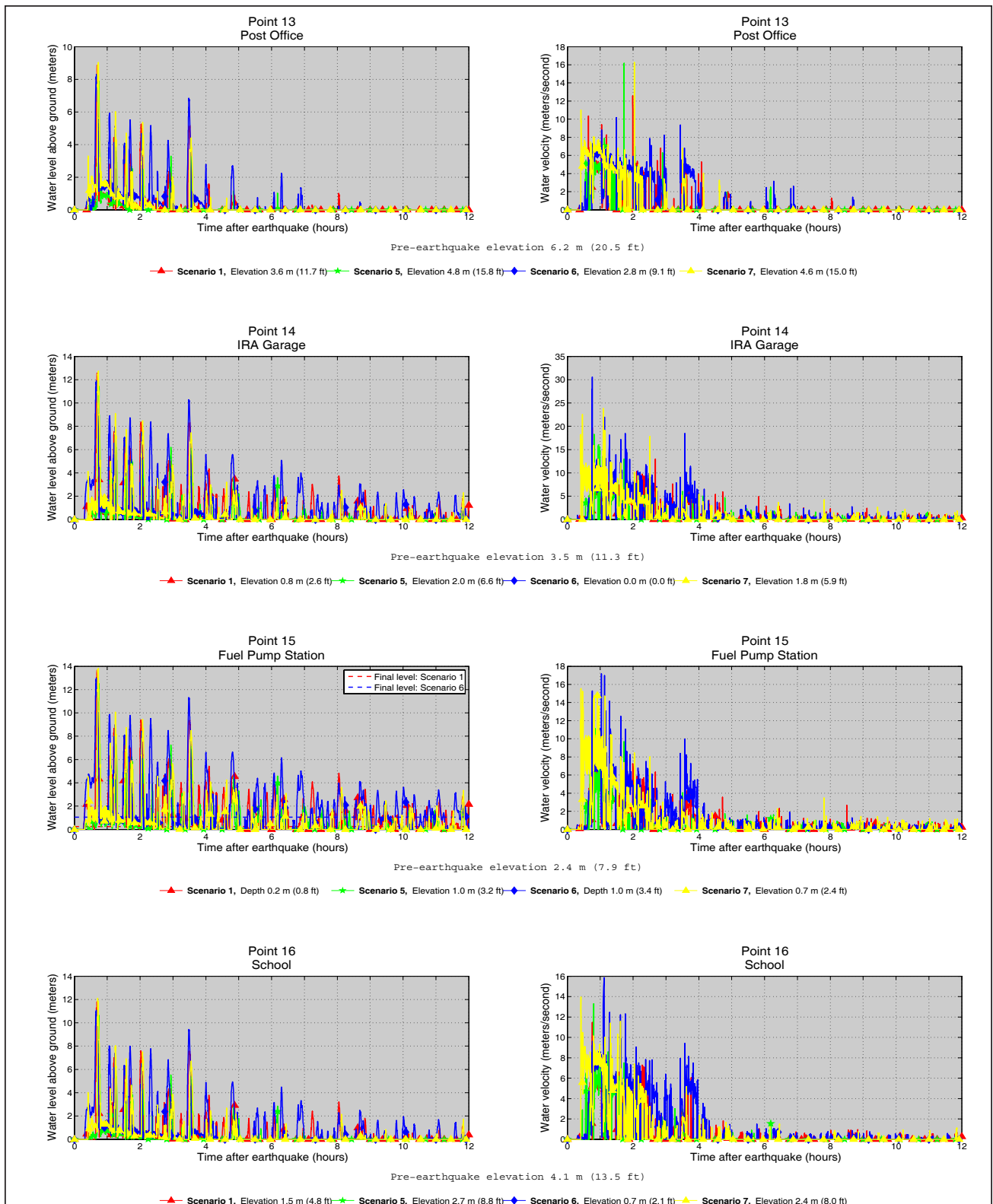
Appendix A-2. Time series of water level (left) and velocity (right) at selected locations in Nikolski and the Pacific coast of Umnak Island for scenarios 1, 5, 6, and 7. The pre-earthquake elevation/depth with respect to the MHHW is stated for each location. The post-earthquake elevation/depth corresponding to the MHHW datum is also listed for each scenario. For offshore locations, to show the height of an arriving tsunami, the vertical datum is such that zero corresponds to the pre-earthquake sea level. The dashed lines show the water level after the tsunami.



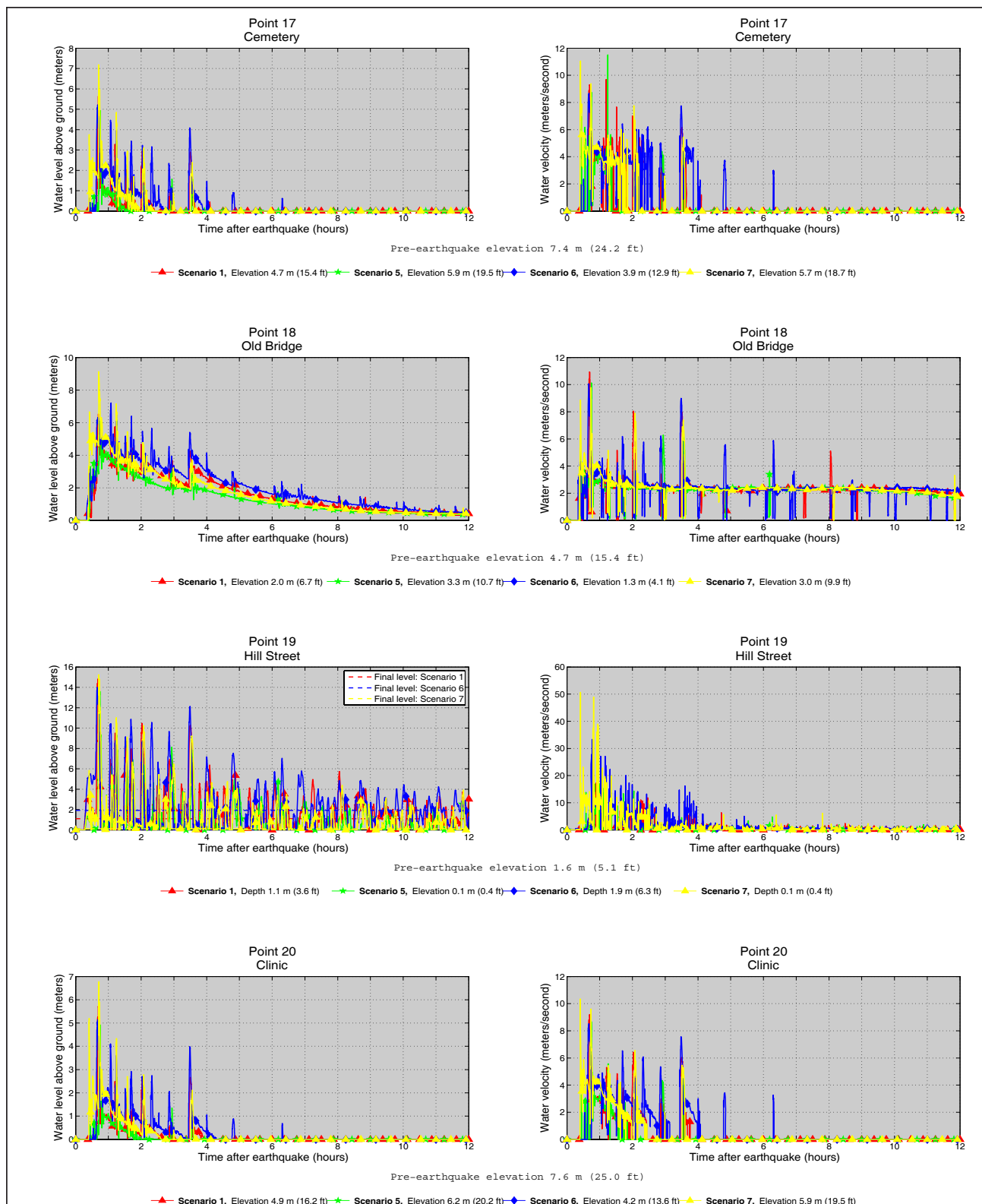
Appendix A-2, continued. Time series of water level (left) and velocity (right) at selected locations in Nikolski and the Pacific coast of Umnak Island for scenarios 1, 5, 6, and 7. The pre-earthquake elevation/depth with respect to the MHHW is stated for each location. The post-earthquake elevation/depth corresponding to the MHHW datum is also listed for each scenario. For offshore locations, to show the height of an arriving tsunami, the vertical datum is such that zero corresponds to the pre-earthquake sea level. The dashed lines show the water level after the tsunami.



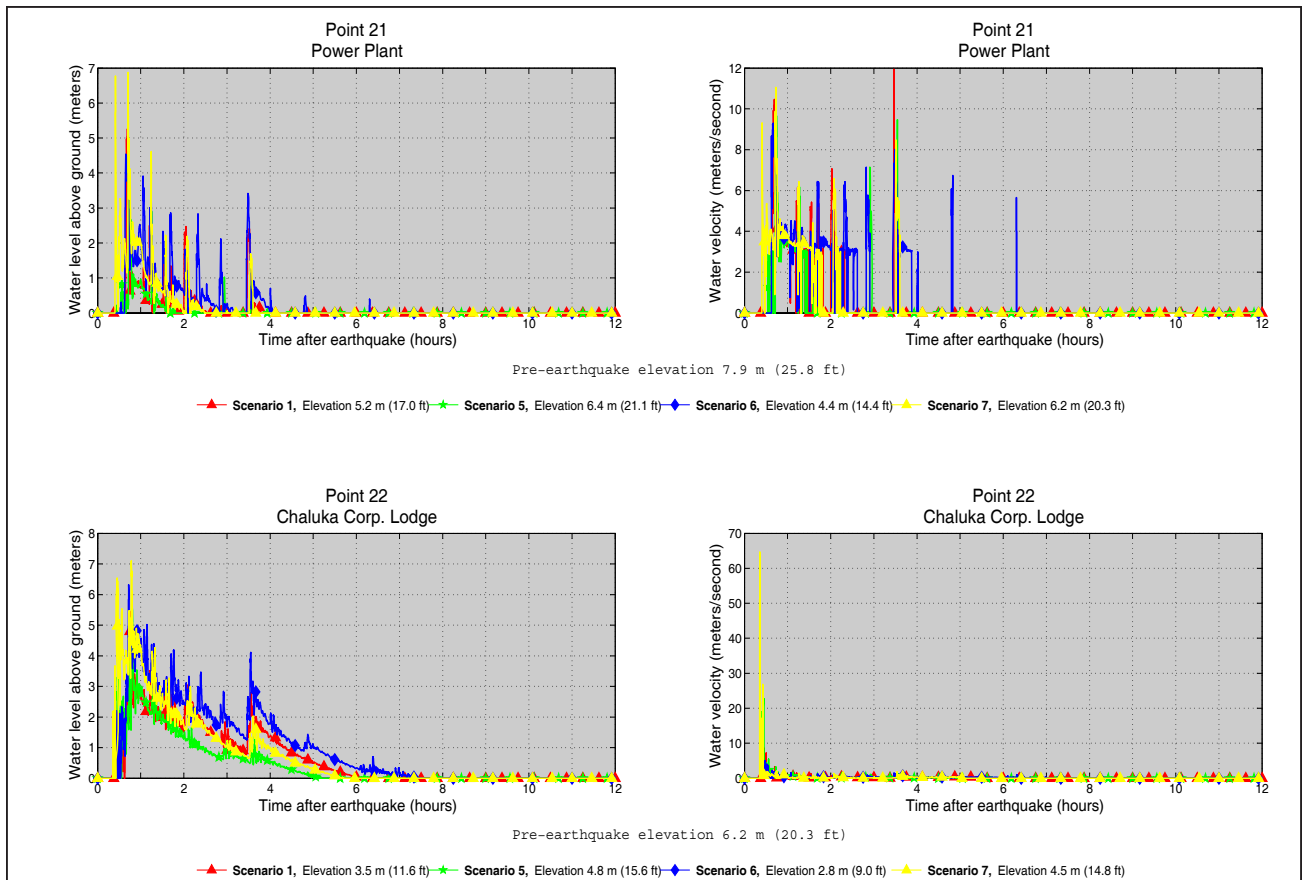
Appendix A-2, continued. Time series of water level (left) and velocity (right) at selected locations in Nikolski and the Pacific coast of Umnak Island for scenarios 1, 5, 6, and 7. The pre-earthquake elevation/depth with respect to the MHHW is stated for each location. The post-earthquake elevation/depth corresponding to the MHHW datum is also listed for each scenario. For offshore locations, to show the height of an arriving tsunami, the vertical datum is such that zero corresponds to the pre-earthquake sea level. The dashed lines show the water level after the tsunami.



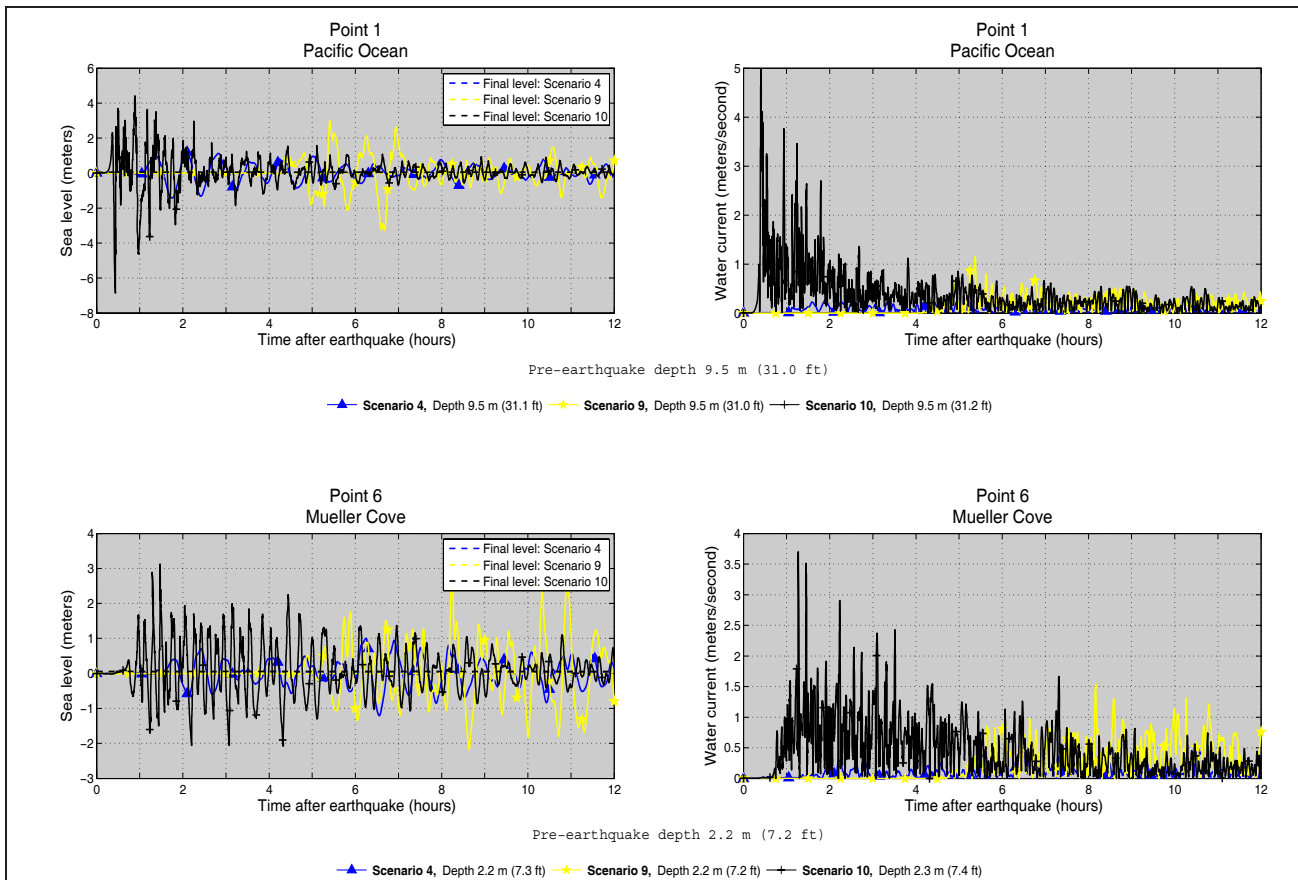
Appendix A-2, continued. Time series of water level (left) and velocity (right) at selected locations in Nikolski and the Pacific coast of Umnak Island for scenarios 1, 5, 6, and 7. The pre-earthquake elevation/depth with respect to the MHHW is stated for each location. The post-earthquake elevation/depth corresponding to the MHHW datum is also listed for each scenario. For offshore locations, to show the height of an arriving tsunami, the vertical datum is such that zero corresponds to the pre-earthquake sea level. The dashed lines show the water level after the tsunami.



Appendix A-2, continued. Time series of water level (left) and velocity (right) at selected locations in Nikolski and the Pacific coast of Umnak Island for scenarios 1, 5, 6, and 7. The pre-earthquake elevation/depth with respect to the MHHW is stated for each location. The post-earthquake elevation/depth corresponding to the MHHW datum is also listed for each scenario. For offshore locations, to show the height of an arriving tsunami, the vertical datum is such that zero corresponds to the pre-earthquake sea level. The dashed lines show the water level after the tsunami.



Appendix A-2, continued. Time series of water level (left) and velocity (right) at selected locations in Nikolski and the Pacific coast of Umnak Island for scenarios 1, 5, 6, and 7. The pre-earthquake elevation/depth with respect to the MHHW is stated for each location. The post-earthquake elevation/depth corresponding to the MHHW datum is also listed for each scenario. For offshore locations, to show the height of an arriving tsunami, the vertical datum is such that zero corresponds to the pre-earthquake sea level. The dashed lines show the water level after the tsunami.



Appendix A-3. Time series of water level (left) and velocity (right) at selected offshore locations in Mueller Cove and along the Pacific coast of Umnak Island for scenarios 4, 9, and 10. The pre-earthquake depth with respect to the MHHW is stated for each location. The post-earthquake depth corresponding to the MHHW datum is also listed for each scenario. For offshore locations, to show the height of an arriving tsunami, the vertical datum is such that zero corresponds to the pre-earthquake sea level. The dashed lines show the water level after the tsunami.

Table A-1. The longitude and latitude locations of the time series points in Nikolski. The maximum water depth above ground is provided for on-shore locations, whereas the maximum water level above the pre-earthquake MHHW is provided for offshore locations. The pre-earthquake onshore (S) and offshore (O) locations are specified in the third column. The minimum elevation above the post-earthquake MHHW datum is provided for onshore locations, while the minimum post-earthquake depth is provided for offshore locations.

#	Label	S / O	Longitude (deg. W)	Latitude (deg. N)	Minimum Elevation/ Depth (m)	Maximum Water Depth Above Ground/Sea Level (m)										Maximum Water Velocity (m/sec)									
						Scenario										Scenario									
						1	2	3	4	5	6	7	8	9	10	1	2	3	4	5	6	7	8	9	10
1	Pacific Ocean	O	168.857778	52.907500	9.4	43.0	42.7	40.4	1.2	55.3	33.4	51.9	18.4	3.0	4.4	8.7	9.2	7.9	0.3	11.3	8.0	11.6	4.5	1.2	5.0
2	Beach on the Pacific side	S	168.864167	52.911111	1.0	31.7	33.4	29.3	0.0	39.7	31.4	41.0	15.4	0.0	3.5	15.1	26.2	17.1	0.0	18.3	15.9	27.9	6.7	0.0	15.9
3	Lake A	S	168.871111	52.912778	2.1	20.4	19.2	19.7	0.0	19.4	20.8	27.0	4.7	0.0	0.0	18.4	44.2	18.9	0.0	22.5	17.4	21.1	9.3	0.0	0.0
4	Lake B	S	168.873056	52.920278	1.1	9.2	9.5	7.7	0.0	12.9	9.0	15.9	1.5	0.0	0.0	15.2	16.5	14.0	0.0	20.0	16.7	20.4	2.4	0.0	0.0
5	Umnak Lake	O	168.860278	52.935556	3.0	10.4	10.2	10.0	0.0	10.4	11.4	15.5	2.4	0.0	0.0	9.1	8.4	9.6	0.0	7.0	8.5	11.8	8.7	0.0	0.0
6	Mueller Cove	O	168.864167	52.940556	2.2	16.0	15.2	16.0	1.0	14.7	15.7	16.5	11.1	2.8	3.1	5.1	4.8	4.9	0.5	5.3	8.1	6.8	5.1	1.5	3.7
7	Umnak Lake Subdivision	S	168.870556	52.938056	12.1	0.6	0.0	0.5	0.0	0.0	0.0	2.1	0.0	0.0	0.0	5.2	0.0	5.2	0.0	0.0	0.0	9.0	0.0	0.0	0.0
8	IRA satellite dishes	S	168.868333	52.938056	4.3	6.8	6.3	6.8	0.0	6.1	6.4	8.5	3.4	0.0	0.0	8.3	12.6	9.2	0.0	7.8	8.6	6.1	4.3	0.0	0.0
9	HUD housing	S	168.870833	52.936111	14.7	0.0	0.0	0.0	0.0	0.0	0.0	0.0	0.0	0.0	0.0	0.0	0.0	0.0	0.0	0.0	0.0	0.0	0.0	0.0	0.0
10	Chaluka Corp. wool shed	S	168.865833	52.938333	0.0	12.0	11.3	11.9	0.0	11.1	11.4	12.9	7.5	0.0	0.0	18.4	16.0	16.9	0.0	16.1	18.0	19.3	5.0	0.0	0.0
11	Main Street	S	168.864167	52.938611	-1.6	14.5	13.9	14.4	0.0	13.5	13.8	15.2	9.6	1.1	1.2	14.8	12.7	9.9	0.0	15.9	10.6	30.7	5.4	1.8	3.6
12	Church	S	168.861667	52.938333	4.2	5.6	5.1	5.5	0.0	4.8	5.1	6.7	2.2	0.0	0.0	9.4	9.1	9.3	0.0	8.8	8.8	12.3	6.3	0.0	0.0
13	Post office	S	168.861389	52.938889	2.8	8.9	8.3	8.8	0.0	7.9	8.3	9.0	4.6	0.0	0.0	12.6	11.5	9.0	0.0	16.2	10.2	16.3	4.5	0.0	0.0
14	IRA Garage	S	168.861111	52.939444	0.0	12.6	11.9	12.5	0.0	11.4	11.9	12.7	7.6	0.0	0.0	19.7	15.1	17.4	0.0	18.3	30.6	23.8	6.9	0.0	0.0
15	Fuel pump station	S	168.860833	52.939722	-1.0	13.7	13.0	13.6	0.0	12.5	13.0	13.8	8.6	0.6	0.9	11.5	9.2	11.5	0.0	11.9	17.2	15.5	2.9	0.7	1.7
16	School	S	168.860278	52.940000	0.7	11.8	11.2	11.8	0.0	10.6	11.1	12.1	6.7	0.0	0.0	11.5	10.5	11.2	0.0	13.3	15.9	14.0	5.5	0.0	0.0
17	Cemetery	S	168.861111	52.938056	3.9	5.6	5.2	5.6	0.0	4.9	5.2	7.2	2.5	0.0	0.0	9.7	11.5	9.9	0.0	11.5	8.7	11.1	5.7	0.0	0.0
18	Old bridge	S	168.862222	52.937500	1.3	6.5	6.2	6.4	0.0	6.2	7.2	9.1	4.7	0.0	0.0	10.9	10.5	10.9	0.0	10.1	10.0	9.8	8.1	0.0	0.0
19	Hill Street	S	168.860278	52.941111	-1.9	14.8	14.1	14.9	0.0	13.6	14.0	15.2	9.0	1.3	1.5	20.4	17.5	17.5	0.0	17.0	33.3	50.7	4.9	0.9	2.8
20	Clinic	S	168.860000	52.938611	4.2	5.7	5.3	5.7	0.0	4.9	5.1	6.8	2.2	0.0	0.0	9.2	8.9	9.1	0.0	8.7	8.5	10.3	5.6	0.0	0.0
21	Power plant	S	168.858056	52.939722	4.4	5.3	4.6	5.3	0.0	4.1	4.5	6.9	1.5	0.0	0.0	11.9	9.9	10.4	0.0	9.7	9.3	11.0	7.3	0.0	0.0
22	Chaluka Corp. Lodge	S	168.870000	52.934444	2.8	5.5	5.3	4.7	0.0	5.7	6.3	7.1	0.0	0.0	0.0	18.9	17.5	12.0	0.0	22.7	14.8	64.6	0.0	0.0	0.0